Available online at www.sciencedirect.com

ScienceDirect

Geochimica et Cosmochimica Acta 218 (2017) 73–97

Geochimica et Cosmochimica Acta

www.elsevier.com/locate/gca

Differentiation and magmatic activity in Vesta evidenced by ^{26}Al-^{26}Mg dating in eucrites and diogenites

G. Hublet [a,1], V. Debaille [a,*], J. Wimpenny [b,2], Q-Z. Yin [b]

[a] *Laboratoire G-Time, Université Libre de Bruxelles, CP 160/02, 50, Av. F.D. Roosevelt, 1050 Brussels, Belgium*
[b] *Department of Earth and Planetary Sciences, University of California at Davis, Davis, CA 95616, USA*

Received 24 November 2016; accepted in revised form 31 August 2017; available online 8 September 2017

Abstract

The ^{26}Al-^{26}Mg short-lived chronometer has been widely used for dating ancient objects in studying the early Solar System. Here, we use this chronometer to investigate and refine the geological history of the asteroid 4-Vesta. Ten meteorites widely believed to come from Vesta (4 basaltic eucrites, 3 cumulate eucrites and 3 diogenites) and the unique achondrite Asuka 881394 were selected for this study. All samples were analyzed for their δ^{26}Mg* and ^{27}Al/^{24}Mg ratios, in order to construct both whole rock and model whole rock isochrons. Mineral separation was performed on 8 of the HED's in order to obtain internal isochrons. While whole rock Al-Mg analyses of HED's plot on a regression that could be interpreted as a vestan planetary isochron, internal mineral isochrons indicate a more complex history. Crystallization ages obtained from internal ^{26}Al-^{26}Mg systematic in basaltic eucrites show that Vesta's upper crust was formed during a short period of magmatic activity at $2.66^{+1.39}_{-0.58}$ million years (Ma) after Calcium-Aluminum inclusions (after CAI). We also suggest that impact metamorphism and subsequent age resetting could have taken place at the surface of Vesta while ^{26}Al was still extant. Cumulate eucrites crystallized progressively from $5.48^{+1.56}_{-0.60}$ to >7.25 Ma after CAI. Model ages obtained for both basaltic and cumulate eucrites are similar and suggest that the timing of differentiation of a common eucrite source from a chondritic body can be modeled at $2.88^{+0.14}_{-0.12}$ Ma after CAI, i.e. contemporaneously from the onset of the basaltic eucritic crust. Based on their cumulate texture, we suggest cumulate eucrites were likely formed deeper in the crust of Vesta. Diogenites have a more complicated history and their ^{26}Al-^{26}Mg systematics show that they likely formed after the complete decay of ^{26}Al and thus are younger than eucrites. This refined chronology for eucrites and diogenites is consistent with a short magma ocean stage on 4-Vesta from which the basaltic eucrites rapidly crystallized. In order to explain the younger age and the complex history of diogenites, we postulate that a second episode of magmatism was possibly triggered by a mantle overturn. We bring a refined chronology of the geological history of Vesta that shows that the asteroid has known a more-complex differentiation than previously thought.
© 2017 The Authors. Published by Elsevier Ltd. This is an open access article under the CC BY license (http://creativecommons.org/licenses/by/4.0/).

Keywords: Al-Mg dating; Vesta; Eucrites; Diogenites

1. INTRODUCTION

Eucrites and diogenites are igneous rocks belonging to the howardite-eucrite-diogenite meteorite (HED) series. The HED's are widely believed to originate from early magmatic activity on the same parent body, one of the three largest asteroids of the asteroid belt, 4-Vesta (Vesta hereafter) (Lugmair and Shukolyukov, 1998; Drake, 2001; Mittlefehldt, 2015). The common origin of these three types

* Corresponding author.
E-mail address: vinciane.debaille@ulb.ac.be (V. Debaille).
[1] Now at National Institute of Polar Research, Tachikawa, Tokyo 190-8518, Japan.
[2] Now at Lawrence Livermore National Laboratory, Livermore, CA 94550, USA.

http://dx.doi.org/10.1016/j.gca.2017.09.005
0016-7037/© 2017 The Authors. Published by Elsevier Ltd.
This is an open access article under the CC BY license (http://creativecommons.org/licenses/by/4.0/).

of achondrite have been confirmed by similarities in their oxygen isotopic composition (Clayton and Mayeda, 1996; Greenwood et al., 2005; Scott et al., 2009; Greenwood et al., 2014). The matching reflectance spectra between HED achondrites and the surface of Vesta suggests that this asteroid is the parent body of HED series (McCord et al., 1970; Consolmagno and Drake, 1977; Pieters et al., 2006). This hypothesis is supported by recent data from the Dawn mission (Russell et al., 2012; McSween et al., 2013; Russell et al., 2013). Large craters observed on the surface of Vesta could be the source of the abundant small objects with identical reflectance spectra found in the asteroid belt called "Vestoids" that could also be the source of HED meteorite found on Earth (Binzel and Xu, 1993), notwithstanding that some eucrites have recently been identified as being anomalous and possibly originated from other parent bodies than Vesta (Scott et al., 2009; Greenwood et al., 2014; Sanborn and Yin, 2014; Williams et al., 2015).

In terms of petrology and mineralogy, eucrites are basaltic to gabbroic achondrites composed of pyroxenes (pigeonite) and plagioclase (Krot et al., 2003). Eucrites can be subdivided into two groups: basaltic (non-cumulate) and cumulate eucrites (Krot et al., 2003). The mineralogy of these two types of eucrite is similar but they have different grain sizes and texture (Krot et al., 2003). Basaltic eucrites are fine to medium grained while cumulate eucrites are characteristically coarse (Krot et al., 2003). The cumulate eucrites can also be distinguished from basaltic eucrites based on chemical features such as higher Mg# (Mg# $\sim$ 57–45 in cumulate eucrites as opposed to Mg# $\sim$ 42–30 in basaltic eucrites), and lower abundance of incompatible trace elements such as LREE (Barrat et al., 2000; Barrat, 2004; Mittlefehldt, 2015). Diogenites are coarser-grained igneous cumulates. These meteorites are orthopyroxenite or harzburgitic achondrites composed of $\sim$90% of orthopyroxene with minor plagioclase and olivine content (Bowman et al., 1997). Assuming that the HED's originated from the same parent body, likely Vesta, they constitute a unique opportunity to investigate early Solar System planetary evolution such as differentiation and early magmatic activity on a large asteroid.

Eucrites and diogenites have traditionally been considered as co-magmatic. As such, different scenarios for their formation have been suggested. First, eucrites are hypothesized to have crystallized from a residual basaltic melt formed by intensive fractional crystallization of a magma ocean. In this case, diogenites, as ultramafic cumulates, would have crystallized directly from the same magma ocean (Righter and Drake, 1997; Ruzicka et al., 1997; Takeda, 1997; Drake, 2001; Greenwood et al., 2005; Larsen et al., 2011; Mandler and Elkins-Tanton, 2013; Greenwood et al., 2014; Mittlefehldt, 2015; Schiller et al., 2017). A second scenario suggests the formation of eucrites and diogenites by partial melting of the Eucrite Parent Body (EPB) with extraction of basaltic magma forming the eucrite crust and crystallization of residual magma forming diogenites (Stolper, 1977; Jones, 1984). However, chemical features such as incompatible trace element abundances suggest no direct link between the two parent magmas of eucrites and diogenites, and also possibly the existence of more than one parental melt for the diogenites (Mittlefehldt, 1994; Fowler et al., 1995; Shearer et al., 1997; Barrat, 2004; Barrat et al., 2008; Mittlefehldt, 2015). In a third scenario, diogenites could have been produced in plutons or in multiple small magma chambers without any genetic relationship with eucrites (Shearer et al., 1997; Barrat et al., 2008; Beck and McSween, 2010; Yamaguchi et al., 2011; Mittlefehldt, 2015). Chemical signatures in some diogenites have been proposed to be crustal contamination (Barrat et al., 2010), originating when diogenites crystallized as intrusions within a eucritic crust. In a fourth scenario, based on oxygen isotope measurements, it has been proposed that diogenites originated from at least two distinct parent bodies (Day et al., 2012). However a careful revaluation of earlier with new oxygen isotopes has concluded to a small variation range for oxygen isotope data between eucrites and diogenites and thus a single parent body (Greenwood et al., 2014). Finally, based on chronological measurements that Vesta formed on a very rapid timescale (within 3 Ma after CAI formation), Schiller et al. (2011) suggested that the HED series may not have originated from Vesta at all, as this asteroid is too large to have such a brief magmatic activity. A similar hypothesis was also considered by Wasson (2013) due to O and Cr isotope data being more similar to the IIIAB asteroid. However, the recent results obtained from the Dawn mission indicate that the surface of Vesta is consistent with the mineralogy of HED meteorites (McSween et al., 2013). If it is assumed that HED meteorites do come from Vesta, their precise dating is of importance to understand the evolution of this asteroid and the possible scenarios of igneous activities related to the formation of eucrites and diogenites. Howardites will not be considered in the following as they are breccia randomly sampling different lithologies and may also record younger impact ages in addition to igneous activity.

Short-lived radioactive-isotope systems are powerful tools to study the early history of the Solar System as they can provide high-resolution age information during the lifetime of their parent isotopes. As such, they serve as the most effective chronometers for the first few million years (Ma) of the Solar System history. However, some inconsistencies exist between different chronometers, and different ages have been proposed for eucrites and diogenites (Table 1). While a pioneering study found no $^{26}Mg^{*}$ in eucrites (Schramm et al., 1970), recent studies have shown that some eucrites have a small excess in $^{26}Mg^{*}$ (Srinivasan et al., 1999; Bizzarro et al., 2005; Schiller et al., 2010a), suggesting the presence of ^{26}Al at the time of their formation. Bizzarro et al. (2005) and Schiller et al. (2010a) showed that asteroidal melting and basaltic magmatism on the EPB occurred $\sim$3 Ma after the Solar System formation. Other dating results obtained on eucrites using ^{53}Mn-^{53}Cr, ^{26}Al-^{26}Mg, ^{60}Fe-^{60}Ni and ^{182}Hf-^{182}W short-lived radioactive systems indicated that core formation and silicate differentiation of Vesta occurred rapidly, 1–5 Ma, after CAI formation (Lugmair and Shukolyukov, 1998; Quitté et al., 2000; Kleine et al.,

Table 1
Age comparison for HED samples between previous studies and this study obtained with different short-lived isotopic system.

Sample	Isotopic system	$(^{26}Al/^{27}Al)_0 \pm 2\sigma$	$\Delta t_{CAI} \pm 2\sigma$	Reference
Basaltic eucrites				
A-881388	^{182}Hf-$^{182}W^z$		$3.97^{+1.10}_{-0.93}$	Srinivasan et al. (2007)
	Pb-Pb^z		47.35 ± 73	Misawa et al. (2005)
A-881467	^{182}Hf-$^{182}W^z$		$6.87^{+2.89}_{-2.19}$	Srinivasan et al. (2007)
	Pb-Pb^z		$15.55^{+16.58}_{-12.02}$	Srinivasan et al. (2004)
	Pb-Pb^z		2.35 ± 10	Misawa et al. (2005)
Agoult	Pb-Pb^z		12.85 ± 2	Iizuka et al. (2015)
Béréba	^{182}Hf-^{182}W		$17.83^{+4.33}_{-3.01}$	Kleine et al. (2005)
	^{182}Hf-^{182}W		$11.13^{+1.35}_{-1.13}$	Touboul et al. (2015)
	Pb-Pb^z		15.35 ± 20	Zhou et al. (2013)
Bouvante	^{182}Hf-^{182}W		$11.25^{+1.09}_{-0.92}$	Touboul et al. (2015)
Cachari	Pb-Pb^z		19.35 ± 24	Zhou et al. (2013)
Caldera	^{53}Mn-^{53}Cr		>21	Lugmair and Shukolyukov (1998)
	Pb-Pb^z		25.35 ± 80	Zhou et al. (2013)
Camel Donga	^{26}Al-^{26}Mg	$2.93 \pm 2.79 \times 10^{-6}$	$\mathbf{3.04^{+3.20}_{-0.70}}$	This study
	^{26}Al-^{26}Mg*	$3.22 \pm 0.42 \times 10^{-6}$	$2.88^{+0.12}_{-0.14}$	Bizzarro et al. (2005)
	^{26}Al-^{26}Mg*	$2.97 \pm 0.61 \times 10^{-6}$	$2.96^{+0.19}_{-0.23}$	Schiller et al. (2010a)
	^{182}Hf-^{182}W		$22.27^{+3.36}_{-2.46}$	Kleine et al. (2005)
	^{182}Hf-^{182}W		$23.09^{+7.71}_{-4.47}$	Touboul et al. (2015)
	Pb-Pb^z		36.35 ± 10	Zhou et al. (2013)
Chervony Kut	^{53}Mn-^{53}Cr		$2.82^{+0.02}_{-0.01}$	Lugmair and Shukolyukov (1998)
Dho 182	^{182}Hf-$^{182}W^z$		9.18 ± 10.62[a]	Roszjar et al. (2016)
EET 87520	^{53}Mn-^{53}Cr		>17	Lugmair and Shukolyukov (1998)
EET 90020	^{182}Hf-$^{182}W^z$		>34.77	Srinivasan et al. (2007)
HaH262	^{26}Al-^{26}Mg*	$1.99 \pm 0.65 \times 10^{-6}$	$3.33^{+0.36}_{-0.24}$	Bizzarro et al. (2005)
HaH286	^{182}Hf-$^{182}W^z$		11.93 ± 3.16[a]	Roszjar et al. (2016)
Ibitira	^{26}Al-^{26}Mg*	$2.46 \pm 0.54 \times 10^{-6}$	$3.11^{+0.20}_{-0.15}$	Bizzarro et al. (2005)
	^{53}Mn-^{53}Cr		$9.50^{+2.81}_{-1.53}$	Lugmair and Shukolyukov (1998)
Juvinas	^{26}Al-^{26}Mg*	$2.78 \pm 0.60 \times 10^{-6}$	$2.99^{+0.20}_{-0.15}$	Bizzarro et al. (2005)
	^{26}Al-^{26}Mg*	$2.62 \pm 0.42 \times 10^{-6}$	$3.05^{+0.13}_{-0.10}$	Schiller et al. (2010a)
	^{182}Hf-^{182}W		$22.22^{+3.56}_{-2.58}$	Kleine et al. (2005)
	^{182}Hf-^{182}W		$22.57^{+2.18}_{-1.72}$	Touboul et al. (2015)
	^{53}Mn-^{53}Cr		$3.94^{+0.38}_{-0.29}$	Lugmair and Shukolyukov (1998)
	Pb-Pb^z		22.35 ± 15	Zhou et al. (2013)
Millbillillie	^{26}Al-^{26}Mg*	$1.62 \pm 0.63 \times 10^{-6}$	$3.54^{+0.46}_{-0.29}$	Bizzarro et al. (2005)
	^{26}Al-^{26}Mg*	$2.39 \pm 0.70 \times 10^{-6}$	$3.14^{+0.30}_{-0.21}$	Schiller et al. (2010a)
NWA 1908	^{182}Hf-$^{182}W^z$		6.50 ± 4.95[a]	Roszjar et al. (2016)
NWA 4523	^{182}Hf-$^{182}W^z$		6.44 ± 3.25[a]	Roszjar et al. (2016)
NWA 5073	^{182}Hf-$^{182}W^z$		20.33 ± 14.41[a]	Roszjar et al. (2016)
NWA 5356	^{182}Hf-$^{182}W^z$		6.09 ± 3.90[a]	Roszjar et al. (2016)
Padvarninkai	Pb-Pb^z		18.35 ± 5	Misawa et al. (2005)
Piplia Kalan	^{26}Al-^{26}Mg	$7.5 \pm 0.9 \times 10^{-7}$	$4.34^{+0.07}_{-0.08}$	Srinivasan et al. (1999)
Pomozdino	Pb-Pb^z		7.35 ± 5	Ireland and Bukovanska (2003)
	^{182}Hf-$^{182}W^z$		$23.24^{+12.96}_{-5.94}$	Ireland and Bukovanska (2003)
Stannern	^{26}Al-^{26}Mg*	$1.26 \pm 0.37 \times 10^{-6}$	$3.80^{+0.31}_{-0.22}$	Bizzarro et al. (2005)
	^{182}Hf-^{182}W		$3.29^{+1.58}_{-1.30}$	Kleine et al. (2005)
	^{182}Hf-^{182}W		$4.32^{+1.77}_{-1.44}$	Touboul et al. (2015)
Y-75011	Pb-Pb^z		15.35 ± 17	Misawa et al. (2005)
Y-792510	Pb-Pb^z		3.35 ± 32	Misawa et al. (2005)

(*continued on next page*)

Table 1 (*continued*)

Sample	Isotopic system	$(^{26}Al/^{27}Al)_0 \pm 2\sigma$	$\Delta t_{CAI} \pm 2\sigma$	Reference
Cumulate eucrites				
Dhofar 007	^{26}Al-^{26}Mg*	$3.06 \pm 0.91 \times 10^{-6}$	$2.89^{+0.31}_{-0.22}$	Bizzarro et al. (2005)
	^{26}Al-^{26}Mg*	$3.32 \pm 1.40 \times 10^{-6}$	$2.80^{+0.51}_{-0.31}$	Schiller et al. (2010a)
Moore County	^{53}Mn-^{53}Cr		>17	Lugmair and Shukolyukov (1998)
Pomozdino	^{53}Mn-^{53}Cr		>12	Lugmair and Shukolyukov (1998)
Serra de Magé	^{53}Mn-^{53}Cr		$13.10^{+2.37}_{-1.36}$	Lugmair and Shukolyukov (1998)
Talampaya	^{26}Al-^{26}Mg*	$2.26 \pm 1.05 \times 10^{-6}$	$3.20^{+0.59}_{-0.34}$	Bizzarro et al. (2005)
Diogenites				
Johnstown	^{26}Al-^{26}Mg	$-4.19 \pm 2.24 \times 10^{-5}$	**>7.25**	This study
	^{53}Mn-^{53}Cr		>6	Lugmair and Shukolyukov (1998)
Shalka	^{53}Mn-^{53}Cr		>10	Lugmair and Shukolyukov (1998)
Whole rocks				
Basaltic eucrite	^{26}Al-^{26}Mg	$4.19 \pm 3.07 \times 10^{-6}$	$\mathbf{2.66^{+1.39}_{-0.58}}$	This study
	^{182}Hf-^{182}W		$3.19^{+0.01}_{-0.01}$	Quitté and Birck (2004)
	^{182}Hf-^{182}W		$11.34^{+1.10}_{-0.93}$	Touboul et al. (2015)
Cumulate eucrite	^{26}Al-^{26}Mg	$0.06 \pm 1.54 \times 10^{-4}$	–	This study
	^{182}Hf-^{182}W		≥27	Touboul et al. (2015)
Eucrite group	^{26}Al-^{26}Mg	$3.06 \pm 0.95 \times 10^{-6}$	$\mathbf{2.99^{+0.39}_{-0.28}}$	This study
	^{182}Hf-^{182}W		$3.81^{+0.33}_{-0.29}$	Kleine et al. (2004)
Diogenite	^{26}Al-^{26}Mg	–	–	This study
Diogenite + mesosiderite	^{53}Mn-^{53}Cr		$2.13^{+0.03}_{-0.03}$	Day et al. (2012)
HED group	^{26}Al-^{26}Mg	$2.78 \pm 1.24 \times 10^{-6}$	$\mathbf{3.09^{+0.62}_{-0.39}}$	This study
	^{53}Mn-^{53}Cr		$1.55^{+0.01}_{-0.01}$	Lugmair and Shukolyukov (1998)
	^{53}Mn-^{53}Cr		$2.13^{+0.03}_{-0.03}$	Trinquier et al. (2008)
Model age				
Eucrite group	^{26}Al-^{26}Mg*	$3.42 \pm 0.43 \times 10^{-6}$	$\mathbf{2.88^{+0.14}_{-0.12}}$	This study
	^{26}Al-^{26}Mg*		2.1–2.8	Schiller et al. (2011)
	^{182}Hf-^{182}W*		$2.86^{+0.62}_{-0.54}$	Kleine et al. (2004)
Diogenite group	^{26}Al-^{26}Mg*	$-0.83 \pm 5.45 \times 10^{-5}$	–	This study
	^{26}Al-^{26}Mg*		2.5	Schiller et al. (2011)

* Model age.
[z] Zircon age.
[a] Average ± 2SD. Δt_{CAI} (in Myr) are obtained using the Efremovka 22E CAI $(^{26}Al/^{27}Al)_0 = 5.25 \pm 0.02 \times 10^{-5}$ (Larsen et al., 2011), CAI value for $(^{182}Hf/^{180}Hf)_0 = 1.018 \pm 0.043 \times 10^{-4}$ (Kruijer et al., 2014) and CAI value for $(^{53}Mn/^{55}Mn)_0 = 6.28 \pm 0.66 \times 10^{-6}$ (Trinquier et al., 2008). For the ^{207}Pb-^{206}Pb isotopic system, Δt_{CAI} are obtained by back calculation of CAI absolute age of 4567.35±0.28 Ma (Connelly et al., 2012). Data in bold are from this study (cfr. Table 3).

2004; Bizzarro et al., 2005; Kleine et al., 2005; Trinquier et al., 2008; Schiller et al., 2010a; Tang and Dauphas, 2012). In contrast, internal ^{53}Mn-^{53}Cr isochrons show a large range of ages that span over 20 Ma (Lugmair and Shukolyukov, 1998). ^{182}Hf-^{182}W isotopic systematics from whole-rock analyses of basaltic and cumulate eucrites gave a crystallization range of ~3 Ma (Yin et al., 2002) to ~10 Ma after CAI formation (Quitté et al., 2000; Quitté and Birck, 2004). ^{182}Hf-^{182}W internal isochrons also show a large range of individual ages for the two types of eucrites, from 4.2 Ma up to 22.8 Ma after CAI formation (Kleine et al., 2005; Touboul et al., 2015). Finally, U-Pb, Pb-Pb and Hf-W dating of zircons in basaltic eucrites suggest that magmatic activity in Vesta persisted up to 50 Ma after CAI formation (Zhou et al., 2013; Roszjar et al., 2016).

Ages for diogenites are even more controversial (Table 1). Some studies have considered diogenites being contemporaneous with or older than eucrites (Trinquier et al., 2008; Schiller et al., 2011). Day et al. (2012) have dated diogenites at 4564.8 ± 0.9 Ma using the short-lived ^{53}Mn-^{53}Cr chronometer. This age corresponds to an isochron defined by diogenites and eucrites but also mesosiderites that are thought to share a genetic link with HED achondrites due to the similar O-isotope and ^{54}Cr and ^{50}Ti of HED and mesosiderites (Stewart et al., 1994; Clayton and Mayeda, 1996; Greenwood et al., 2005; Trinquier et al., 2008), and corresponds approximately to the age of basaltic eucrite formation. However, Lugmair and Shukolyukov (1998) obtained an age of ≤4561 Ma for diogenites, supported by the differentiation model for

Vesta (Neumann et al., 2014) and the diogenite formation model of Barrat et al. (2010). Finally, some long-lived isotopic system such as ^{147}Sm-^{143}Nd and ^{176}Lu-^{176}Hf have also been used to show that basaltic eucrites formed very early after the Solar System formation, ~100 Ma before cumulate eucrites and diogenites (Blichert-Toft et al., 2002).

As illustrated above, the chronology of eucrites and diogenites is poorly constrained and the magmatic connection between eucrites and diogenites is unclear, with some studies considering them to be co-magmatic (belonging to the same isochron) (e.g. Day et al., 2012; Schiller et al., 2017) while some others not (e.g. Barrat et al., 2008; Mittlefehldt, 2015). Here, we investigate in detail the temporal relationship between eucrites and diogenites by comparing internal (mineral separates), external (whole rock -WR-) as well as model (compared to a chondritic starting composition) ^{26}Al-^{26}Mg isochrons in order to enhance our understanding of the geological history of Vesta. The ^{26}Al-^{26}Mg isotopic system is of particular interest because of its high temporal resolution, its high abundance (Al and Mg being both major elements) and its resistance to resetting due to the relatively high closure temperature of the system (LaTourrette and Wasserburg, 1998). The now extinct radionuclide ^{26}Al decayed to ^{26}Mg with a half-life of 0.73 Ma (Walker et al., 1989). This chronometer can thus date only the objects that formed during a period of <5 Ma after the Solar System formation. Any object that formed during this period with a fractionated Al/Mg ratio relative to the estimated bulk chondritic value (~0.101) (Scott and Krot, 2003) will present an anomaly in $\delta^{26}Mg^*$ that is expressed as a deviance from the terrestrial mass-dependent average value. The deviation from the reference terrestrial value is noted $\delta^{26}Mg^*$, and is expressed as:

$$\delta^{26}Mg^* = \delta^{26}Mg - [(1 + 0.001 \times \delta^{25}Mg)^{1/0.511} - 1] \times 1000 \quad (1)$$

In this study, only monomict specimens have been selected to constrain the timing of differentiation and the magmatic history of Vesta. For this, we analyzed 4 basaltic eucrites (Camel Donga, Millbillillie, Yamato (Y-)792510, Y-793591), 3 cumulate eucrites (Yamato (Y-)980318, Y-980433 and Asuka (A-)881819) and 3 diogenites (Bilanga, Johnstown and Tatahouine). Finally, in order to reinvestigate its relationship with the EPB, we also analyzed the A-881394 unique achondrite that was considered as a cumulate eucrite based on its mineralogy but excluded from the HED group because of its O, Cr and Ti isotope signatures not consistent with the group (Scott et al., 2009; Greenwood et al., 2014; Sanborn and Yin, 2014; Williams et al., 2015). Six of these samples were obtained from the Antarctic meteorite collection of National Institute of Polar Research in Japan (NIPR) (Y-792510, Y-793591, Y-980318, Y-980433, A-881819 and A-881394). Four samples (Millbillillie, Bilanga, Johnstown and Tatahouine) were obtained from the meteorite collection of the Royal Belgian Institute for Natural Sciences in Brussels, Belgium. A piece of Camel Donga was obtained commercially.

2. ANALYTICAL TECHNIQUES

Preparation and chemical procedures were performed in a clean laboratory at the Université Libre de Bruxelles (ULB). Each sample was cleaned in an ultrasonic bath with trace grade acetone. Then, ~50 mg of each sample was crushed in an agate mortar for bulk rock analyzes. Mineral separation was performed on ~200–500 mg fractions of six eucrites (Camel Donga, Y-792510, Y-793591, Y-980433, Y-980318 and A-881819), of two diogenites (Bilanga and Johnstown) and of the A-881394 achondrite. The samples were crushed and sieved between 64 and 125 μm. The different mineral fractions were obtained from density separation using heavy liquids (methylene iodide) and then by magnetic separation on a Frantz magnetic separator. In the case of diogenites, as they are mostly composed of orthopyroxene, all the mineral fractions (Fr.) will be orthopyroxene with small variation in their chemical composition (e.g. Mittlefehldt, 2015).

Around 50 mg of bulk-rock samples and the available mass of mineral fractions were dissolved in an HNO_3/HF (2:1) mixture followed by two steps in concentrated HNO_3. After complete dissolution, an aliquot of 0.5% was taken for measuring ^{27}Al/^{24}Mg ratios. Magnesium was separated using cation-exchange resin (BIO Rad AG®50W-X12, 100–200 mesh) following the procedure in Jacobsen et al. (2008). The purification procedure consists of loading an aliquot of 20 μl of the dissolved sample followed by three successive steps on the same column (0.4 cm diameter × 10 cm length) using 18 ml of 1N HNO_3. The only difference with the procedure from Jacobsen et al. (2008) is the use of a mixture of 1N HNO_3:0.1N HF during the second step to ensure a complete removing of Ti from the Mg fraction as observed by Schiller et al. (2010b). While this procedure ensures the total removal of Ti and Fe and better than 99.9% and 99.7% of Al and Ca respectively, the Mg yield was checked and was better than 90% over the full procedure. Blank contribution was negligible.

Mg isotopic ratios of eucrites and diogenites were measured on the HR-MC-ICP-MS Nu-Plasma at the ULB using an Aridus 2 desolvating nebulizer. Samples were introduced in 0.05 N HNO_3. Measurements were performed in medium resolution in order to avoid possible isobaric interferences (e.g. ^{12}C^{14}N) (Jacobsen et al., 2008). No other major interference was observed. The instrumental mass bias was corrected by exponential law (reflected in the exponent of 0.511 in Eq. (1)) (Wasserburg et al., 2012) and sample-standard bracketing with the DSM-3 Mg isotope standard (Galy et al., 2003). Each standard and sample measurement consisted of a cycle of three blocks of 20 measurements with a concentration of ~400 ppb, corresponding to ~7.5–8 V on ^{24}Mg. Some Mg isotope data were also collected using the new HR-MC-ICP-MS Nu-Plasma II at ULB using an Apex desolvating nebulizer. Analyzes were also performed in medium resolution with the same method for the sample introduction and correction. The integration time was 10 s. Each analysis of

Table 2
$^{27}Al/^{24}Mg$ and $\delta^{26}Mg^*$ results for the different samples analyzed in this study.

Sample	$^{27}Al/^{24}Mg \pm 2$ se	$\delta^{26}Mg^* \pm 2$ se (‰) ULB (Nu-plasma I)	$\delta^{26}Mg^* \pm 2$ se (‰) ULB (Nu-plasma II)	$\delta^{26}Mg^* \pm 2$ se (‰) UCDavis (Neptune)	$\delta^{26}Mg^* \pm 2$ se (‰) All data combined
Basaltic eucrites					
Millbillillie WR	1.407 ± 0.008	0.027 ± 0.031 *(3)*		0.032 ± 0.010 *(8)*	0.030 ± 0.010*(11)*
Camel Donga WR	1.412 ± 0.018	0.020 ± 0.014 *(4)*		0.030 ± 0.012 *(7)*	0.026 ± 0.009 *(11)*
px.	0.995 ± 0.013	0.018 ± 0.031 *(5)*		0.025 ± 0.014 *(8)*	0.022 ± 0.014 *(13)*
px-pl.	1.798 ± 0.028	0.038 ± 0.015 *(5)*		0.038 ± 0.012 *(8)*	0.038 ± 0.009 *(13)*
Y-792510 WR	1.365 ± 0.019	0.029 ± 0.009 *(17)*		0.042 ± 0.007 *(6)*	0.032 ± 0.007 *(23)*
px.1	0.105 ± 0.008	0.036 ± 0.015 *(3)*		0.038 ± 0.011 *(5)*	0.037 ± 0.008 *(8)*
px.2	0.146 ± 0.025	0.068 ± 0.020 *(4)*		0.038 ± 0.011 *(10)*	0.046 ± 0.012 *(14)*
pl.[2]	42.567 ± 2.220		0.064 ± 0.023 *(2)*		0.064 ± 0.023 *(2)*
Y-793591 WR	1.031 ± 0.019	0.023 ± 0.008 *(6)*		0.014 ± 0.009 *(5)*	0.019 ± 0.006 *(11)*
px.1	0.240 ± 0.018	0.013 ± 0.007 *(4)*		0.016 ± 0.010 *(6)*	0.015 ± 0.006 *(10)*
px.2	0.555 ± 0.032	0.019 ± 0.028 *(4)*			0.019 ± 0.028 *(4)*
px-pl.	1.924 ± 0.015	0.026 ± 0.006 *(3)*		0.027 ± 0.003 *(5)*	0.026 ± 0.003 *(8)*
Cumulate eucrites					
Y-980318 WR	0.586 ± 0.010	0.009 ± 0.008 (1)		0.010 ± 0.004 *(7)*	0.010 ± 0.003 *(8)*
px.1	0.027 ± 0.001	−0.004 ± 0.012 *(19)*			−0.004 ± 0.012 *(19)*
px.2	0.190 ± 0.006	0.001 ± 0.013 *(11)*			0.001 ± 0.013 *(11)*
pl.[2]	92.823 ± 1.690		0.022 ± 0.005 *(2)*		0.022 ± 0.005 *(2)*
Y-980433 WR	0.453 ± 0.008	0.026 ± 0.023 *(8)*		0.012 ± 0.016 *(4)*	0.021 ± 0.016 *(12)*
px.1	0.040 ± 0.003	0.020 ± 0.005 *(3)*		0.020 ± 0.008 *(5)*	0.020 ± 0.005 *(8)*
px.2	0.143 ± 0.005	0.016 ± 0.013 *(18)*		0.011 ± 0.012 *(7)*	0.015 ± 0.010 *(25)*
pl.[2]	95.064 ± 0.981		0.084 ± 0.006*(2)*		0.084 ± 0.006*(2)*
A-881819 WR	0.657 ± 0.004	0.030 ± 0.012 *(1)*		0.017 ± 0.006 *(8)*	0.018 ± 0.006 *(9)*
Fr 1 (heavy px.)	0.279 ± 0.004	−0.006 ± 0.046 (3)	0.040 ± 0.036 *(5)*		0.022 ± 0.031 *(8)*
Fr.2 (< 0.45 A)	0.709 ± 0.022		0.040 ± 0.018 *(4)*		0.040 ± 0.018 *(4)*
Fr.3 (0.45 to 0.65 A)	0.939 ± 0.007	0.024 ± 0.030 *(7)*	0.049 ± 0.011 *(4)*		0.033 ± 0.020 *(11)*
Fr 4 (0.65 to 0.75 A)	1.775 ± 0.024		0.052 ± 0.031 *(6)*		0.052 ± 0.031 *(6)*
Fr.5 (0.75 to 1.1 A)	2.884 ± 0.027	0.019 ± 0.018 *(3)*	0.047 ± 0.022 *(5)*		0.036 ± 0.018 *(8)*
Fr.6 (> 1.1 A)	9.495 ± 0.199		0.039 ± 0.013 *(7)*		0.039 ± 0.013 *(7)*
Diogenites					
Bilanga WR	0.025 ± 0.003	−0.002 ± 0.005 *(9)*			−0.002 ± 0.005 *(9)*
Fr.1 (HD, < 0.45 A)	0.027 ± 0.006	−0.020 ± 0.007 *(4)*			−0.020 ± 0.007 *(4)*
Fr.2 (HD, 0.45 to 0.50 A)	0.026 ± 0.002	−0.030 ± 0.017 *(13)*			−0.030 ± 0.017 *(13)*
Fr.3 (HD, > 0.50 A)	0.036 ± 0.004	0.001 ± 0.021 *(13)*			0.001 ± 0.021 *(13)*
Fr.4 (LD, < 0.45 A)	0.020 ± 0.002	−0.013 ± 0.031 *(7)*			−0.013 ± 0.031 *(7)*
Fr.5 (LD, 0.45 to 0.50 A)	0.022 ± 0.002	0.008 ± 0.006 *(5)*			0.008 ± 0.006 *(5)*
Fr.6 (LD, > 0.50 A)	0.058 ± 0.004	0.007 ± 0.014 *(6)*			0.007 ± 0.014 *(6)*
Johnstown WR	0.032 ± 0.002	0.019 ± 0.013 *(9)*			0.019 ± 0.013 *(9)*
Fr.1 (HD, < 0.40 A)	0.052 ± 0.008	0.019 ± 0.009 *(7)*			0.019 ± 0.009 *(7)*
Fr.2 (HD, 0.40 to 0.45 A)	0.035 ± 0.003	0.044 ± 0.013 (2)			0.044 ± 0.013 (2)
Fr.3 (HD, > 0.45 A)	0.039 ± 0.002	0.019 ± 0.031 *(5)*			0.019 ± 0.031 *(5)*
Fr.4 (LD, < 0.45 A)	0.063 ± 0.006	0.008 ± 0.034 *(6)*			0.008 ± 0.034 *(6)*
Fr.5 (LD, 0.45 to 0.50 A)	0.035 ± 0.002	0.023 ± 0.003 *(3)*			0.023 ± 0.003 *(3)*
Fr.6 (LD, > 0.50 A)	0.114 ± 0.010	0.000 ± 0.013 *(11)*			0.000 ± 0.013 *(11)*
Tatahouine WR	0.022 ± 0.007	0.012 ± 0.012 *(12)*			0.012 ± 0.012 *(12)*
Fr.1 (HD, < 0.30 A)	0.084 ± 0.004	−0.035 ± 0.001 *(2)*			−0.035 ± 0.001 *(2)*
Fr.2 (HD, 0.30 to 0.40 A)	0.067 ± 0.004	−0.025 ± 0.022 *(4)*			−0.025 ± 0.022 *(4)*
Fr.3 (HD, 0.40 to 0.45 A)	0.060 ± 0.008	−0.016 ± 0.046 *(5)*			−0.016 ± 0.046 *(5)*
Fr.4 (HD, > 0.45 A)	0.058 ± 0.033	0.011 ± 0.013 *(4)*			0.011 ± 0.013 *(4)*
Fr.5 (LD, < 0.30 A)	0.056 ± 0.021	0.019 ± 0.004 *(3)*			0.019 ± 0.004 *(3)*
Fr.6 (LD, 0.30 to 0.40 A)	0.022 ± 0.002	−0.030 ± 0.003 *(2)*			−0.030 ± 0.003 *(2)*
Fr.7 (LD, 0.40 to 0.45 A)	0.020 ± 0.001	−0.022 ± 0.011 *(3)*			−0.022 ± 0.011 *(3)*
Fr.8 (LD, > 0.45 A)	0.043 ± 0.003	0.021 ± 0.035 *(5)*			0.021 ± 0.035 *(5)*
A-881394 achondrite					
A-881394 WR	0.932 ± 0.007		0.076 ± 0.020 *(6)*		0.076 ± 0.020 *(6)*
px.1	0.060 ± 0.001		0.074 ± 0.015 *(6)*		0.074 ± 0.015 *(6)*
px.2	0.099 ± 0.001		0.070 ± 0.023 *(5)*		0.070 ± 0.023 *(5)*
px-pl.	3.866 ± 0.032		0.115 ± 0.025 *(6)*		0.115 ± 0.025 *(6)*

Table 2 (*continued*)

Sample	$^{27}Al/^{24}Mg \pm 2$ se	$\delta^{26}Mg^* \pm 2$ se (‰) ULB (Nu-plasma I)	$\delta^{26}Mg^* \pm 2$ se (‰) ULB (Nu-plasma II)	$\delta^{26}Mg^* \pm 2$ se (‰) UCDavis (Neptune)	$\delta^{26}Mg^* \pm 2$ se (‰) All data combined
pl.	32.995 ± 0.764		0.871 ± 0.135 *(5)*		0.871 ± 0.135 *(5)*
Terrestrial rock					
BCR-2	2.661 ± 0.036				0.005 ± 0.009 *(51)*

The last column is the average of all measurements made on 1 or 2 instruments in this study. The numbers in brackets are the numbers of measurements N. All the data with their full range of digits are presented in Appendix A.
Diogenite fractions correspond to different mineral fraction separated by heavy liquid (high and low densities (respectively HD and LD) compared to 3.3 g/ml) and magnetic field. For BCR, the average value is a combination of both Nu-Plasma I and II measurements.

standards and samples consisted of a cycle of three blocks of 20 measurements with a concentration of ~200 ppb, corresponding to ~20 V on ^{24}Mg. The accuracy and reproducibility of Mg measurements on the two different Nu-Plasma instruments was assessed by repeated measurements of synthetic standard Cambridge 1 (Galy et al., 2003) and a terrestrial rock sample standard (BCR-2) during each session. For the calculation of ^{26}Mg radiogenic excess ($^{26}Mg^*$), $^{26}Mg/^{24}Mg$ values are normalized to $^{25}Mg/^{24}Mg = 0.12663$ (Catanzaro and Murphy, 1966) assumed for the DSM 3 standard (Galy et al., 2003). All the ratios are expressed in ‰ (Eq. (2)), where x stands for ^{25}Mg, ^{26}Mg.

$$\delta^x Mg = \left[\left(\frac{(^xMg/^{24}Mg)_{sample}}{(^xMg/^{24}Mg)_{DSM3}}\right) - 1\right] * 10^3 \quad (2)$$

Isochrons are built as a correlation between $\delta^{26}Mg^*$ (Eq. (1)) and $27Al/^{24}Mg$. All data are presented in Table 2. The $\delta^{26}Mg^*$ value of the BCR-2 terrestrial standard was 0.005 ± 0.009‰ ($n = 51$). Following the approach of Schiller et al. (2011), each $\delta^{26}Mg^*$ value is an average result of 4–12 individual measurements. All the errors reported in the manuscript are 2 times the standard error (2 se).

Measurements of some eucrites were replicated using a Thermo Neptune MC-ICP-MS at University of California in Davis (UC Davis), using the chemical purification procedure from Jacobsen et al. (2008). In this case, samples were introduced in 2% HNO_3 using an Apex IR nebulizer, and each analysis consisted of 20 cycles with 8s integration time. Measurements of sample and standard were made with a concentration of 300 ppb (~30 Von ^{24}Mg). Data are presented in Table 2.

$^{27}Al/^{24}Mg$ ratios for each bulk rock and mineral fraction were measured on an ICP-MS Agilent 7700 at the ULB on aliquots collected from the main dissolution batch without any chemical purification. For the duplicates performed at UC Davis, the $^{27}Al/^{24}Mg$ ratios were measured directly on the MC-ICP-MS Neptune. The $^{27}Al/^{24}Mg$ ratios were calibrated using different standard solutions gravimetrically prepared with different Al/Mg ratios representing the range measured in the present study (Al:Mg of 0:1; 0.01:1; 0.1:1; 2:1; 3:1 and 100:1). Each $^{27}Al/^{24}Mg$ ratio is the average of 5 individual measurements and the quoted errors are the 2 se of those measurements.

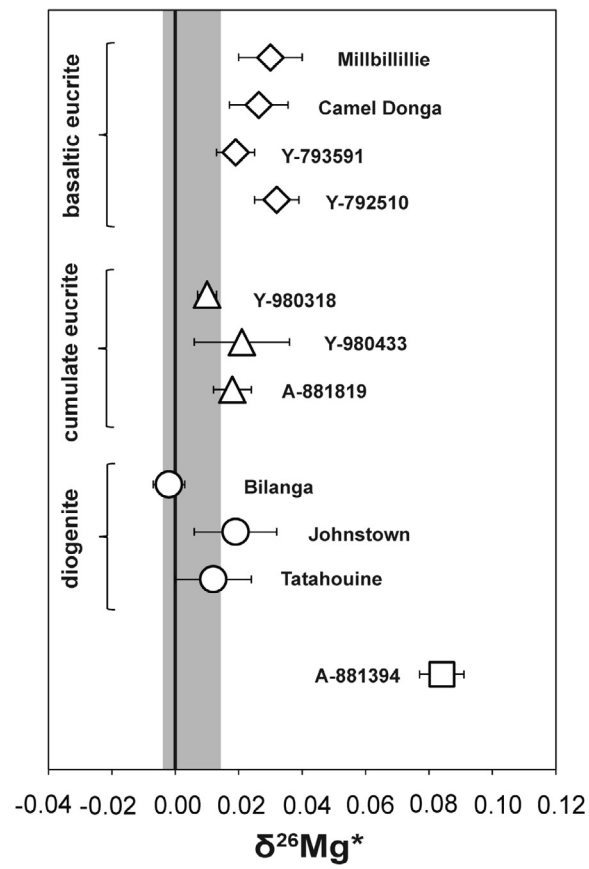

Fig. 1. $\delta^{26}Mg^*$ whole rock values for eucrites, diogenites and A-881394 in this study. The grey zone represents the terrestrial standard value (0.005 ± 0.009, 2 se). Open diamonds are the WR basaltic eucrite samples, open triangles are WR cumulate eucrite samples, open circles are WR diogenite samples and open square is WR A-881394 achondrite. The same legend is used for all diagrams. Error bars are 2 se.

3. RESULTS

All the results for the $^{27}Al/^{24}Mg$ and $\delta^{26}Mg^*$ of each samples of eucrites and diogenites analyzed in this study are presented in Table 2.

Table 3
ages obtained with the ^{26}Al-^{26}Mg isotopic system on the different HED meteorites analyzed in this study.

Samples	$(^{26}Al/^{27}Al)_0 \pm 2\sigma$	$\delta^{26}Mg^*_0 \pm 2\sigma$	$\Delta t_{CAI} \pm 2\sigma$	$T_a \pm 2\sigma$	$T_b \pm 2\sigma$	$T_c \pm 2\sigma$
Basaltic eucrites						
Camel Donga	$2.93 \pm 2.79 \times 10^{-6}$	-0.001 ± 0.030	$3.04^{+3.20}_{-0.70}$	$4564.31^{+0.98}_{-3.48}$	$4565.50^{+0.88}_{-3.38}$	$4565.23^{+0.82}_{-3.32}$
Y-792510	$8.66 \pm 7.54 \times 10^{-8}$	0.036 ± 0.005	$6.75^{+2.15}_{-0.66}$	$4560.60^{+0.94}_{-2.43}$	$4561.79^{+0.84}_{-2.33}$	$4561.52^{+0.78}_{-2.27}$
Y-793591	$1.01 \pm 0.53 \times 10^{-6}$	0.012 ± 0.006	$4.17^{+0.79}_{-0.44}$	$4563.18^{+0.72}_{-1.07}$	$4564.37^{+0.63}_{-0.96}$	$4564.10^{+0.57}_{-0.91}$
Cumulate eucrites						
Y-980318	$2.07 \pm 3.35 \times 10^{-8}$	0.009 ± 0.012	>7.25	–	–	–
Y-980433	$9.60 \pm 1.13 \times 10^{-8}$	0.019 ± 0.004	$6.64^{+0.13}_{-0.11}$	$4560.71^{+0.39}_{-0.41}$	$4561.90^{+0.30}_{-0.31}$	$4561.63^{+0.24}_{-0.25}$
A-881819	$2.89 \pm 2.24 \times 10^{-7}$	0.021 ± 0.006	$5.48^{+1.56}_{-0.60}$	$4561.87^{+0.88}_{-1.84}$	$4563.06^{+0.78}_{-1.74}$	$4562.79^{+0.72}_{-1.68}$
Diogenites						
Bilanga	$-0.14 \pm 2.37 \times 10^{-4}$	0.000 ± 0.047	–	–	–	–
Johnstown	$-4.19 \pm 2.24 \times 10^{-5}$	0.034 ± 0.007	–	–	–	–
Tatahouine	–	–	–	–	–	–
Whole rock						
Basaltic eucrite (n = 4)	$4.19 \pm 3.07 \times 10^{-6}$	-0.012 ± 0.028	$2.66^{-1.39}_{-0.58}$	$4564.69^{+0.86}_{-1.67}$	$4565.88^{+0.76}_{-1.57}$	$4565.60^{+0.70}_{-1.51}$
Cumulate eucrite (n = 3)	$0.06 \pm 1.54 \times 10^{-4}$	-0.012 ± 0.660	–	–	–	–
Eucrite group (n = 7)	$3.06 \pm 0.95 \times 10^{-6}$	-0.001 ± 0.006	$2.99^{+0.39}_{-0.28}$	$4564.36^{+0.56}_{-0.67}$	$4565.54^{+0.46}_{-0.57}$	$4565.27^{+0.40}_{-0.51}$
Diogenite (n = 3)	–	–	–	–	–	–
HED group (n = 10)	$2.78 \pm 1.24 \times 10^{-6}$	0.001 ± 0.007	$3.09^{+0.62}_{-0.39}$	$4564.26^{+0.67}_{-0.90}$	$4565.44^{+0.57}_{-0.80}$	$4565.17^{+0.51}_{-0.74}$
A-881394 achondrite	$2.98 \pm 1.54 \times 10^{-6}$	0.063 ± 0.031	$3.02^{+0.76}_{-0.43}$	$4564.33^{+0.71}_{-1.04}$	$4565.52^{+0.62}_{-0.94}$	$4565.24^{+0.56}_{-0.88}$
Model ages						
Basaltic eucrites	$3.32 \pm 0.47 \times 10^{-6}$	-0.004 ± 0.001	$2.91^{+0.16}_{-0.14}$	$4564.44^{+0.42}_{-0.44}$	$4565.63^{+0.32}_{-0.34}$	$4565.36^{+0.26}_{-0.28}$
Cumulate eucrites	$3.80 \pm 3.21 \times 10^{-6}$	-0.004 ± 0.006	$2.77^{+1.96}_{-0.64}$	$4564.58^{+0.92}_{-2.24}$	$4565.77^{+0.82}_{-2.14}$	$4565.50^{+0.76}_{-2.08}$
Eucrite group	$3.42 \pm 0.43 \times 10^{-6}$	-0.004 ± 0.001	$2.88^{+0.14}_{-0.12}$	$4564.47^{+0.40}_{-0.42}$	$4565.66^{+0.30}_{-0.32}$	$4565.39^{+0.24}_{-0.26}$
Diogenites	$-0.83 \pm 5.45 \times 10^{-5}$	0.004 ± 0.034	–	–	–	–
HED group	$3.34 \pm 0.87 \times 10^{-6}$	-0.003 ± 0.003	$2.90^{+0.31}_{-0.24}$	$4564.45^{+0.52}_{-0.59}$	$4565.64^{+0.42}_{-0.49}$	$4565.36^{+0.36}_{-0.43}$

Δt_{CAI} and ages T_a are obtained using the Efremovka 22E CAI ($(^{26}Al/^{27}Al)_0 = 5.25 \pm 0.02 \times 10^{-5}$ for an absolute age of 4567.35 ± 0.28 Ma; (Larsen et al., 2011; Connelly et al., 2012) as anchor value. Ages T_b are obtained using the angrite D'Orbigny ($(^{26}Al/^{27}Al)_0 = 3.88 \pm 0.27 \times 10^{-7}$ for an absolute age of 4563.37 ± 0.25 Ma; (Schiller et al., 2010a; Brennecka and Wadhwa, 2012) and ages T_c using a CAI of NWA 2364 CV3 chondrite ($(^{26}Al/^{27}Al)_0 = 5.03 \pm 0.26 \times 10^{-5}$ for an absolute age of 4568.22 ± 0.17 Ma; (Bouvier and Wadhwa, 2010). The ages used in the present manuscript are Δt_{CAI} and ages T_a. Age in bracket indicates a non-resolvable $(^{26}Al/^{27}Al)_0$. Model ages have been calculated using the $^{27}Al/^{24}Mg$ and $\delta^{26}Mg^*$ of the non-CAI-bearing chondrites (0.091 ± 0.002 and -0.0015 ± 0.0013 respectively; (Schiller et al., 2010b; Baker et al., 2012).

3.1. $^{27}Al/^{24}Mg$ and $\delta^{26}Mg^*$ on HED and A-881394 achondrite

Basaltic eucrites: Four basaltic eucrites have been analyzed in this study (Millbillillie, Camel Donga, Y-792510 and Y-793591). The whole rock (WR) basaltic eucrite have a supra-chondritic $^{27}Al/^{24}Mg$ ratio (1.031 ± 0.019 to 1.412 ± 0.018), compared to the chondritic value of 0.091 ± 0.002 (Schiller et al., 2010b; Baker et al., 2012). The values of $\delta^{26}Mg^*$ range between 0.019 ± 0.006 and 0.032 ± 0.007 (Fig. 1). All these meteorites present a fully resolvable excess in $\delta^{26}Mg^*$ from the terrestrial standard (0.005 ± 0.009), except Y-793591. Three basaltic eucrites were selected for mineral separation (Camel Donga, Y-792510 and Y-793591). All the mineral separates (pyroxene (px), plagioclase (pl) or mixed fractions (px-pl)) of these three meteorites present a fully resolvable excess in $\delta^{26}Mg^*$ (0.026 ± 0.009–0.064 ± 0.023), except the two pyroxene fractions of Y-793591 and the pyroxene fraction of Camel Donga with values of 0.015 ± 0.006, 0.019 ± 0.028 and 0.022 ± 0.014 respectively that fall within error in the terrestrial range.

Cumulate eucrites: The 3 cumulate eucrites (A-881819, Y-980318 and Y-980433) have supra-chondritic whole rock $^{27}Al/^{24}Mg$ ratios (0.453 ± 0.008–0.657 ± 0.004). These samples have a value of $\delta^{26}Mg^*$ (0.010 ± 0.003–0.021 ± 0.016) close to or within the terrestrial range (Fig. 1) Mineral separation has been performed on all three cumulate eucrites. Almost all mineral separates have a supra-chondritic (0.143 ± 0.005–95.064 ± 0.981) value for the $^{27}Al/^{24}Mg$ ratios. Only the two px.1 fractions from both Y-980318 and Y-980433 have a sub-chondritic value (respectively 0.027 ± 0.001 and 0.040 ± 0.003). The $\delta^{26}Mg^*$ values for mineral fractions fall within the range of the terrestrial value, except for fractions 2, 5 and 6 of A-881819 (0.040 ± 0.018, $0.036 \pm 0.018 \pm 0.003$ and 0.039 ± 0.013) and the pl. fractions of Y-980318 (0.022 ± 0.005) and Y-980433 (0.084 ± 0.006).

Diogenites: The three diogenites analyzed (Bilanga, Johnstown and Tatahouine) have sub-chondritic $^{27}Al/^{24}Mg$

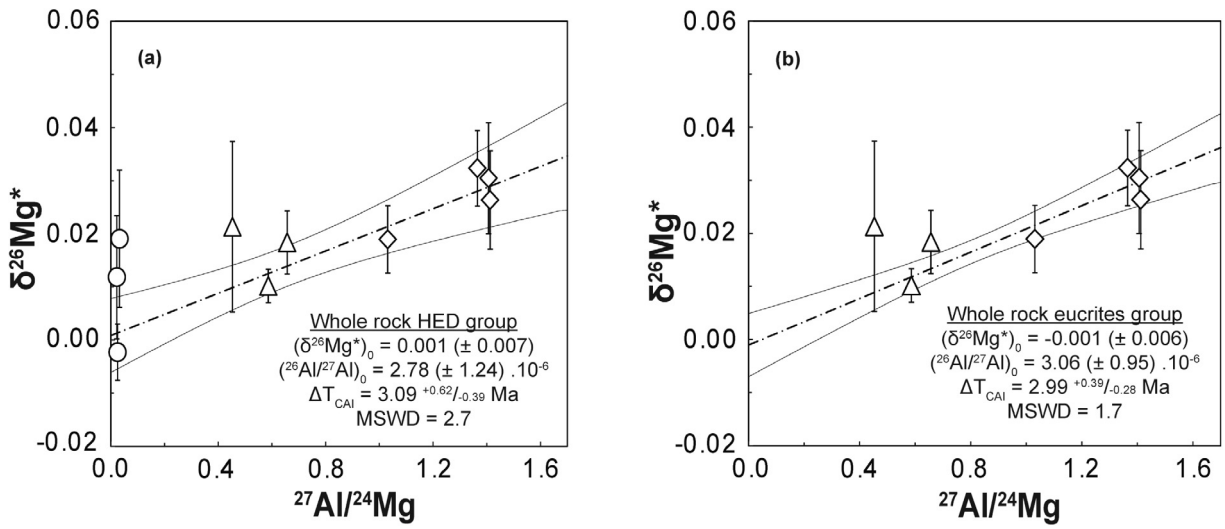

Fig. 2. (a) WR regression (dashed line) of all meteorites of the HED group ($n = 10$; errorchron in the 95% confidence interval, see (Mahon, 1996) for a comprehensive discussion about MSDW and isochron interpretation); (b) WR regression (dashed line) of the two eucrites group analyzed in this study ($n = 7$; isochron in the 95% confidence interval). Calculations made using the Isoplot software (Ludwig, 2012). The solid lines are the 2σ error envelop.

ratios (0.025 ± 0.003–0.032 ± 0.002) for whole rock. Mineral separates was performed on these three diogenites. The $^{27}Al/^{24}Mg$ ratios of mineral fractions have also sub-chondritic values (0.020 ± 0.001–0.084 ± 0.0084), except fraction 6 of Johnstown (0.114 ± 0.010). The $\delta^{26}Mg^*$ values of the whole rock and mineral fractions are within the terrestrial range, but two Bilanga mineral fractions (fraction 1 and 2 with -0.020 ± 0.007 and -0.030 ± 0.017 respectively) and Tatahouine mineral fractions (fractions 1, 6 and 7 with -0.035 ± 0.001, -0.030 ± 0.003 and -0.022 ± 0.011 respectively) show a fully resolvable negative anomaly (Table 2). Only two mineral fractions (fractions 2 and 5) in Johnstown diogenite show a fully resolvable positive anomaly in ^{26}Mg corresponding respectively to a $\delta^{26}Mg^*$ of 0.044 ± 0.013 and 0.023 ± 0.003.

A-881394 achondrite: Almost all fractions and the whole rock of this achondrite have supra-chondritic $^{27}Al/^{24}Mg$ ratios (0.932 ± 0.007–32.995 ± 0.764). Only two fractions of pyroxene present a sub-chondritic value or in the range of chondritic value (0.060 ± 0.001 and 0.099 ± 0.001). The $\delta^{26}Mg^*$ values of the whole rock and mineral fractions present large positive anomalies (0.070 ± 0.023–0.871 ± 0.135).

3.2. $^{26}Al/^{26}Mg$ crystallization age

In order to gain absolute age significance, ^{26}Al-^{26}Mg data must be anchored to an absolute timescale, typically an object that has both well-defined ^{26}Al-^{26}Mg systematics and has been dated with high precision using the Pb-Pb system. In this study we have investigated three objects as age anchors. The first is the Efremovka 22E CAI dated by ^{235}U-corrected Pb-Pb systematic at 4567.35 ± 0.28 Ma (Connelly et al., 2012) and having an $(^{26}Al/^{27}Al)_0$ of $5.25 \pm 0.02 \times 10^{-5}$ (Larsen et al., 2011). The second object is the quenched angrite D'Orbigny with an absolute ^{235}U-corrected Pb-Pb age of 4563.37 ± 0.25 Ma (Brennecka and Wadhwa, 2012) and an $(^{26}Al/^{27}Al)_0$ of $3.88 \pm 0.27 \times 10^{-7}$ (Schiller et al., 2010a). Finally, the third object is the type B CAI of NWA 2364 CV3 chondrite with a Pb-Pb absolute age of 4568.22 ± 0.17 Ma and a $(^{26}Al/^{27}Al)_0$ of $5.03 \pm 0.26 \times 10^{-5}$ (Bouvier and Wadhwa, 2010). We chose not to use this last anchor because the Pb-Pb age has not been ^{235}U-corrected. The second anchor, D'Orbigny, can be younger than some of the samples analyzed here and we also decided not using this anchor. In the present study, we have thus expressed both relative and absolute ages using the Efremovka CAI. The results are presented in Table 3. All $(^{26}Al/^{27}Al)_0$ ratios have been calculated assuming uncorrelated errors between $^{27}Al/^{24}Mg$ and $\delta^{26}Mg^*$ and using the Isoplot software considering the model 1 fit (Ludwig, 2012).

Whole rock HED: whole rock regressions combining all groups of HED meteorites analyzed in this study have also been constructed. The initial value of $(^{26}Al/^{27}Al)_0 = 2.78 \pm 1.24 \times 10^{-6}$ (Fig. 2a) for HED group (errorchron, combining the two types of eucrites and diogenites) and $3.06 \pm 0.95 \times 10^{-6}$ (Fig. 2b) for eucrite group (isochron, combining basaltic and cumulate eucrites) are obtained. These values correspond respectively to the relative ages of $3.09^{+0.62}_{-0.39}$ Ma and $2.99^{+0.39}_{-0.28}$ Ma after CAI. Using the Efremovka 22E CAI anchor value, it can be translated to an absolute age of $4564.26^{+0.67}_{-0.90}$ Ma for HED group and $4564.36^{+0.56}_{-0.67}$ Ma for eucrite group.

Basaltic eucrites: The three basaltic eucrites Camel Donga, Y-792510 and Y-793591 have initial $(^{26}Al/^{27}Al)_0$ ratios of $2.93 \pm 2.79 \times 10^{-6}$ (Fig. 3a), $8.66 \pm 7.54 \times 10^{-8}$ (Fig. 3b) and $1.01 \pm 0.53 \times 10^{-6}$ (Fig. 3c), respectively.

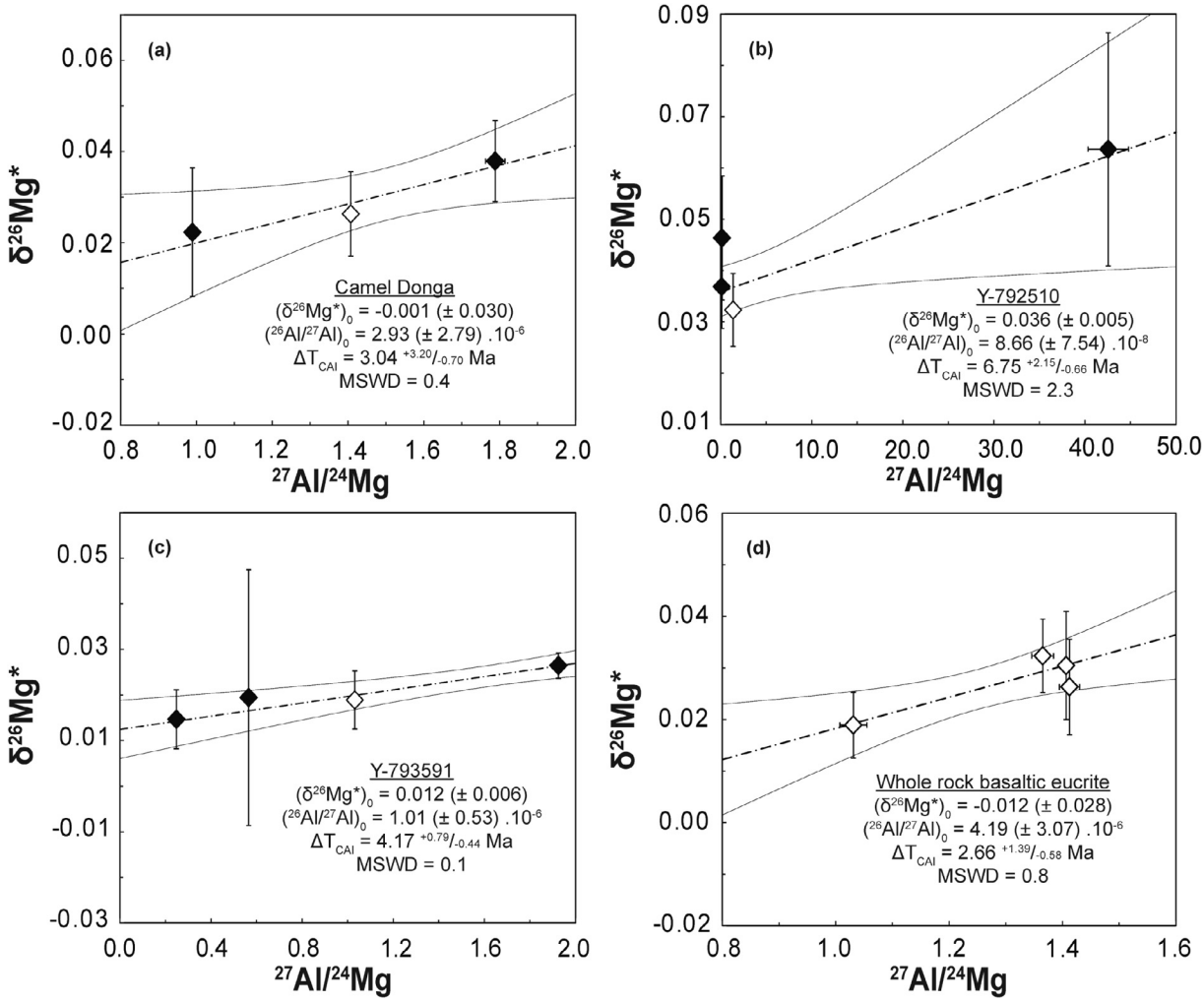

Fig. 3. Internal regressions (dashed lines) prepared on mineral separates of 3 basaltic eucrites: (a) Camel Donga ($n = 3$, isochron in the 95% confidence interval), (b) Y-792510 ($n = 4$, isochron in the 95% confidence interval) and (c) ($n = 4$, isochron in the 95% confidence interval); (d) WR regression of basaltic eucrites ($n = 4$, isochron in the 95% confidence interval). Calculations made using Isoplot software (Ludwig, 2012). Open symbols are WR values and black symbols are mineral fraction values. The solid lines are the 2σ error envelop.

The relative ages of these basaltic eucrites obtained by internal isochrons correspond to $3.04^{+3.20}_{-0.70}$ Ma after CAI for Camel Donga, $6.75^{+2.15}_{-0.66}$ Ma after CAI for Y-792510, and $4.17^{+0.79}_{-0.44}$ Ma after CAI for Y-793591 respectively (Fig. 3a –c). These relative ages can be translated to an absolute age of $4564.31^{+0.98}_{-3.48}$ Ma (Camel Donga), $4560.60^{+0.94}_{-2.43}$ (Y-792510) and $4563.18^{+0.72}_{-1.07}$ (Y-793591) using the Efremovka 22E CAI anchor value. If we regress the 4 basaltic eucrites WR data (Camel Donga, Y-793591, Y-792510 and Millbillillie) (Fig. 3d), we obtain a resolvable initial $(^{26}Al/^{27}Al)_0$ ratio of $4.19 \pm 3.07 \times 10^{-6}$ which gives a relative WR ^{26}Al-^{26}Mg crystallization age of $2.66^{+1.39}_{-0.58}$ Ma after CAI corresponding to an absolute age of $4564.69^{+0.86}_{-1.67}$ Ma using the same anchor as before.

Cumulate eucrite: The three cumulate eucrites Y-980318, Y-980433 and A-881819 have initial $(^{26}Al/^{27}Al)_0$ ratios of $2.07 \pm 3.35 \times 10^{-8}$ (Fig. 4a), $9.60 \pm 1.13 \times 10^{-8}$ (Fig. 4b), and $2.89 \pm 2.24 \times 10^{-7}$ (Fig. 4c) respectively. Only the two last cumulate eucrites have a resolvable $(^{26}Al/^{27}Al)_0$ value which gives a relative ^{26}Al-^{26}Mg crystallization age of $6.64^{+0.13}_{-0.11}$ Ma after CAI for Y-980433 and $5.48^{+1.56}_{-0.60}$ Ma after CAI for A-881819, and only A-881819 gives a statistically meaningful isochron. These two relative ages can be translated to an absolute age of $4560.71^{+0.39}_{-0.41}$ Ma (Fig. 4b) and $4561.87^{+0.88}_{-1.84}$ Ma (Fig. 4c). Even if the $(^{26}Al/^{27}Al)_0$ is not fully resolvable for Y-980318, we can estimate the relative age for this sample corresponding to >7.25 Ma after CAI. It should be noted that Y-980318 and Y-980433 are thought to be paired based on petrological observations, but their ^{26}Al-^{26}Mg crystallization ages do not overlap within 2σ error.

Diogenite: A regression can be obtained only for two diogenites (Bilanga and Johnstown). The data obtained

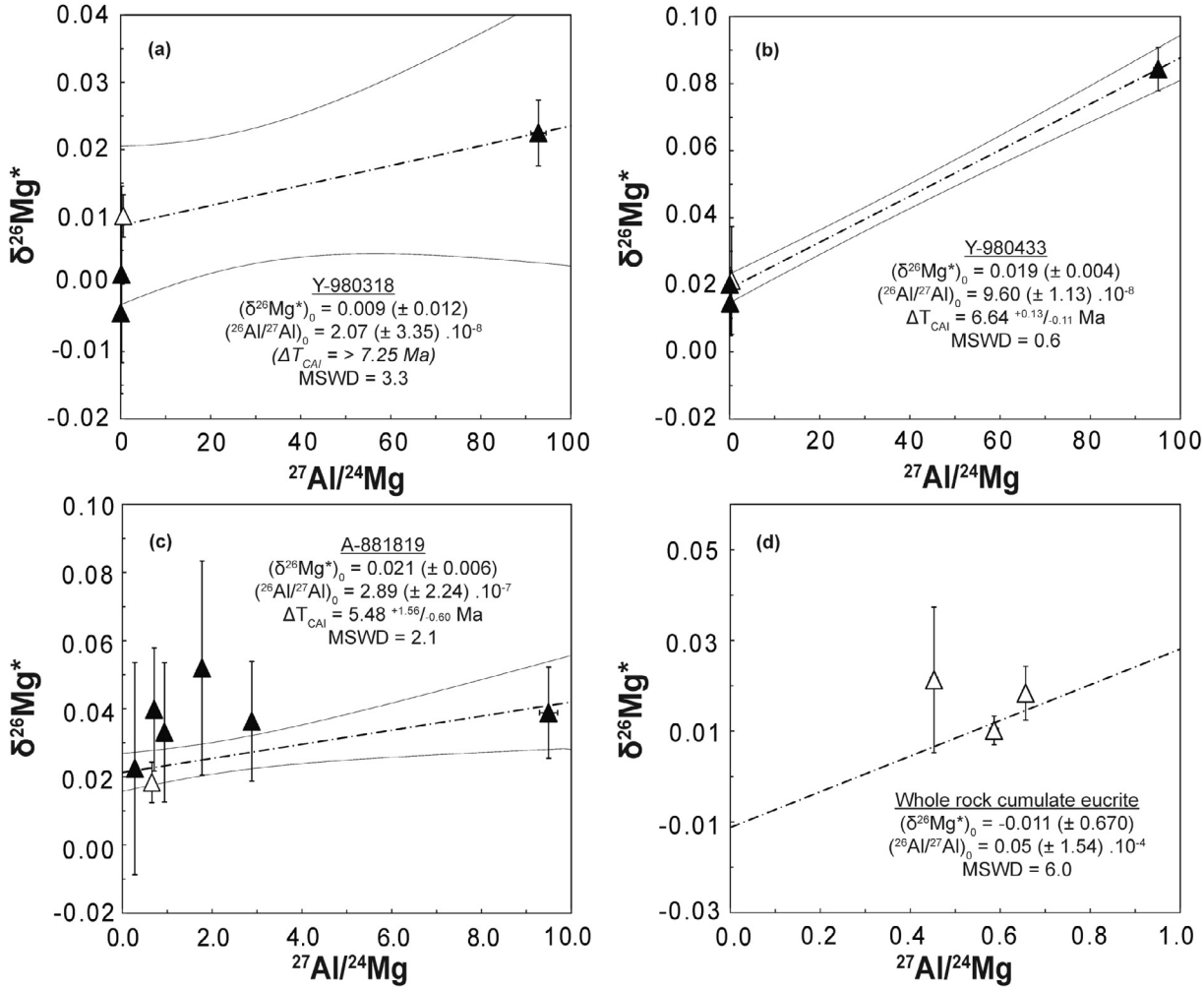

Fig. 4. Internal regressions (dashed lines) prepared on mineral separates of the 3 cumulate eucrites: (a) Y-980318 ($n = 4$, errorchron and non-resolvable $(^{26}Al/^{27}Al)_0$), (b) Y-980433 ($n = 4$, isochron in the 95% confidence interval) and (c) A-881819 ($n = 7$, isochron in the 95% confidence interval); (d) WR regression of all cumulate eucrites ($n = 3$, errorchron and non-resolvable $(^{26}Al/^{27}Al)_0$). Open symbols are WR values and black symbols are mineral fraction values. Calculations made using the Isoplot software (Ludwig, 2012). The solid lines are the 2σ error envelop.

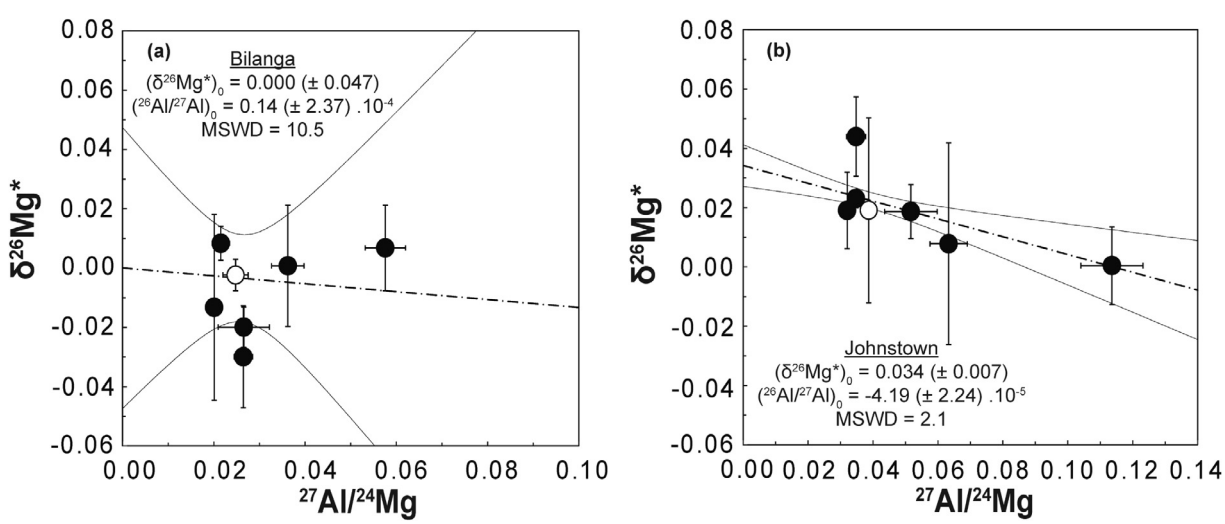

Fig. 5. Internal regressions (dashed lines) prepared on mineral separates of 2 diogenites (a) Bilanga ($n = 7$; errorchron and non-resolvable $(^{26}Al/^{27}Al)_0$) and (b) Johnstown ($n = 7$, meaningful regression but negative initial $(^{26}Al/^{27}Al)_0$). Open symbols are WR values and black symbols are mineral fraction values. Calculations made using the Isoplot software (Ludwig, 2012). The solid lines are the 2σ error envelop.

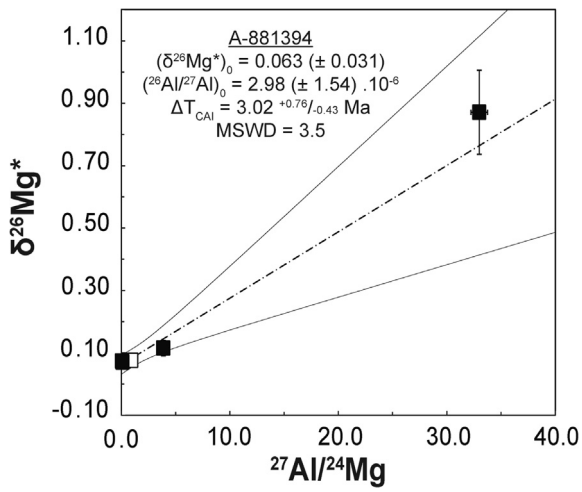

Fig. 6. Internal regression (dashed lines) prepared on mineral separates of the A-881394 achondrite analyzed in this study ($n = 5$, errorchron in the 95% confidence interval). Open symbols are WR values and black symbols are mineral fraction values. Calculations made using the Isoplot software (Ludwig, 2012). The solid lines are the 2σ error envelop.

for the Tatahouine diogenite does not define any correlation and cannot be drawn. Initial $(^{26}Al/^{27}Al)_0$ ratios of Bilanga and Johnstown correspond respectively to $-0.14 \pm 2.37 \times 10^{-4}$ and $-4.19 \pm 2.24 \times 10^{-5}$ and do not define isochrons (Fig. 5a and b). The Johnstown regression is negatively resolvable from 0, but this result cannot be considered as it is not geologically acceptable. The WR ^{26}Al-^{26}Mg data does not define any isochron either.

A-881394 achondrite: an internal errorchron for A-881394 yields an initial $(^{26}Al/^{27}Al)_0$ value of $2.98 \pm 1.54 \times 10^{-6}$ (Fig. 6). Relative age of this sample is $3.02^{+0.76}_{-0.43}$ Ma after CAI and the corresponding absolute age is $4564.33^{+0.71}_{-1.04}$ Ma using the Efremovka 22E CAI.

4. DISCUSSION

4.1. Whole rock HED isochron: A planetary isochron?

A traditional investigation, when working with samples thought to come from a single planetary body, is to plot all the samples together on a single 'planetary' isochron. If an asteroid has a simple geological history, all the samples should provide evidence for the same differentiation and crystallization event. However, while statistical and mathematical tools can easily identify a robust linear correlation, it is still important to interpret the geological meaning of this relationship. This can be done with external parameters related to the geological context of the samples. For example, a ^{142}Nd-^{143}Nd linear relationship between the martian meteorite group of shergottites has been variously interpreted as a simple mixing line between planetary reservoirs without chronological meaning (Debaille et al., 2007) or as a planetary isochron indicating the global differentiation of Mars (Caro et al., 2008). This kind of uncertainty is probably related to one of two explanations. The first is that the analytical uncertainty could cause some details to be hidden. The samples providing the greatest dispersion on the isochron will actually control the whole regression, while its associated error will also be controlled by individual errors. As such, samples could randomly plot on an isochron even though they are not co-genetic or contemporaneous. The supplementary error added by considering those samples will simply be included within the error of the regression, and only the geological context can help distinguishing the two data sets. The second explanation is related to the mixing between two ancient reservoirs within the planetary body, as the mixing line between those two reservoirs will evolve with time. Over a period of time relatively long compared to the half-life of the parent element, the mixing line between these ancient reservoirs will evolve to give an age that is potentially close to the average differentiation age of the body (e.g. Nebel et al., 2014). In this case, even though the two ages could be very close, they reflect different geological processes in terms of planetary differentiation. Planetary isochrons should thus be interpreted with caution, and additional information is certainly needed in order to accurately interpret their meaning.

Despite basaltic and cumulate eucrites differing in terms of certain chemical and mineralogical features (Barrat et al., 2000; Barrat, 2004), they have previously been considered to have formed at the same time (Bizzarro et al., 2005; Schiller et al., 2010a; Day et al., 2012). Previous studies using ^{53}Mn-^{53}Cr systematics also suggested that diogenites have the same age as eucrites (Trinquier et al., 2008; Day et al., 2012). Based on this assumption, a ^{26}Al-^{26}Mg HED WR regression could be constructed to evaluate their time of formation that gives an errorchron with a relative age of $3.09^{+0.62}_{-0.39}$ Ma after CAI (Fig. 2a). This age is consistent with previous relative ages of 2.3 ± 1.3 Ma after CAI (Trinquier et al., 2008), 3.20 ± 0.65 Ma after CAI obtained for all HED samples (Wimpenny et al., 2011) and the range of 2–3 Ma after CAI evaluated by Day et al. (2012). The first simple explanation would be that Vesta underwent a major differentiation event and very rapidly crystallized to generate eucrites and diogenites. On the other hand, plotting only eucrites together (Fig. 2b) gives a similar relative age of $2.99^{+0.39}_{-0.28}$ Ma after CAI, but now with an isochron associated to better statistics (MSWD of 1.7 instead of 2.7 for all HED). Finally, plotting only basaltic eucrites gives an isochron with a relative age of $2.66^{-1.39}_{-0.58}$ Ma after CAI with a slightly larger error but a better MSWD of 0.8 (Fig. 3d). This last age is also identical to the two previous ages, but slightly more robust in terms of statistics. Observing 3 times the same age when working with basaltic eucrites could imply that the HED isochron is actually controlled by basaltic eucrites. In this case, plotting cumulate eucrites and diogenites on this isochron does not improve the quality of the isochron itself. It is thus important now to evaluate in detail if cumulate eucrites and diogenites actually belong to the basaltic eucrite isochron by looking at the internal isochrons.

4.2. Detailed chronology of ED

4.2.1. ^{26}Al-^{26}Mg age of eucrites

As previously said basaltic and cumulate eucrites share mineralogical characteristics but are slightly distinct in their chemical composition. While both cumulate and basaltic eucrites seem to define an isochron at $2.99^{+0.39}_{-0.28}$ Ma after CAI (Fig. 2b), the WR basaltic eucrites define by themselves an isochron at $2.66^{+1.39}_{-0.58}$ Ma after CAI (Fig. 3d) (i.e. similar within error). In contrast, the regression of WR cumulate eucrites does not define an isochron (Fig. 4d).

When looking in more detail at mineral-separate isochrons, two of the three basaltic eucrites (Camel Donga and Y-793591) have similar crystallization relative ages of $3.04^{+3.20}_{-0.70}$ and $4.17^{+0.79}_{-0.44}$ Ma after CAI,. There is thus a good agreement between the external isochron obtained using the 4 basaltic eucrites (including Millbillillie WR) and those two internal isochrons, reinforcing the interpretation that basaltic eucrites likely crystallized from a single short event that can be constrained. As such, only the basaltic eucrite WR age of $2.66^{+1.39}_{-0.58}$ Ma after CAI will be considered for basaltic eucrites in the following discussion. The Y-792510 internal isochron show a younger age of $6.75^{+2.15}_{-0.66}$ Ma after CAI. The case of this basaltic eucrite will be discussed in the next section, because there is strong evidence to suggest that its internal age was reset. In any case, this younger internal age does not prevent Y-792510 to plot well on the $2.66^{-1.39}_{-0.58}$ Ma after CAI basaltic eucrite isochron.

The ages obtained for cumulate eucrites by internal isochrons span from $5.48^{+1.56}_{-0.60}$ Ma to >7.25 Ma after CAI, thus resolvably younger than the WR basaltic eucrite age, even though the individual crystallization ages of basaltic eucrites overlap within error with the cumulate eucrite internal age. These results show that for the samples considered here, cumulate eucrites are actually younger than basaltic eucrites, implying that plotting both cumulate and basaltic eucrites together on the same isochron may be mathematically acceptable, but cannot be justified from a geological point of view. The age difference between basaltic and cumulate eucrites agrees with thermal modeling (Neumann et al., 2014) that suggested that basaltic eucrites formed prior to cumulate eucrites and diogenites.

Observations and results from the Dawn mission have shown that the outer part of Vesta crust is mostly composed of basaltic lava flows (McSween et al., 2013) confirming the hypothesis of Takeda (1997) and Nyquist et al. (1997). Our data for basaltic eucrites indicate that extrusive magmatic activity on Vesta has occurred at $2.66^{+1.39}_{-0.58}$ after CAI, in agreement with some previous ^{26}Al-^{26}Mg and ^{53}Mn-^{53}Cr dating (Lugmair and Shukolyukov, 1998; Srinivasan et al., 1999; Nyquist et al., 2003; Bizzarro et al., 2005; Trinquier et al., 2008). The younger age of cumulate eucrites can be explained by slow cooling deeper in the crust of Vesta (Barrat et al., 2010) until the complete extinction of ^{26}Al. Thermal models suggest that ^{26}Al and possibly ^{60}Fe decay are the heat source for asteroidal magmatism and differentiation (Ghosh and McSween, 1998; Bizzarro et al., 2005; Sahijpal et al., 2007) within 3–4 Ma after CAI. Ages obtained for the basaltic eucrites (Srinivasan et al., 1999; Nyquist et al., 2003; Bizzarro et al., 2005; Schiller et al., 2010a; this study) are consistent with this hypothesis, implying that crystallization occurred while ^{26}Al was still present. In addition, core-mantle segregation and accumulation of ^{26}Al into the mantle could have kept the interior of an asteroid such as Vesta warm for a longer time period, up to 7–8 Ma after CAI (Sahijpal et al., 2007). Our results for cumulate eucrites suggest that they crystallized close to and/or just after the complete extinction of ^{26}Al (>7.25 Ma after CAI for Y-980318). These data are also in agreement with thermal modeling (Neumann et al., 2014). Such a protracted period is at odds with the study of Schiller et al. (2011) where they estimated by mathematical modeling crystallization ages of 2–3 Ma after CAI for both cumulate and basaltic eucrites. They thus suggested that eucrites did not originate from Vesta, as an asteroid the size of Vesta should have experienced a relatively longer magmatic history. However, Schiller et al. (2011) did their modeling on only one basaltic eucrite (Juvinas) and one cumulate eucrite (Dho007), the former being considered as anomalous (Yamaguchi et al., 2006). Their modeled age agrees well with the age obtained here for basaltic eucrites. On the other hand, the crystallization ages obtained for cumulate eucrites in the present study effectively extend the duration of the magmatic activity on Vesta, and thus do not prevent a vestan origin, following the argument of Schiller et al. (2011).

Recent studies have proposed that Vesta could have had an even more prolonged magmatic history than evidence from the present study suggests. Based on zircon U-Pb and Pb-Pb dating in basaltic eucrites (see compilation in Table 1), Zhou et al. (2013) suggested that Vesta underwent a peak of basaltic magmatism at 4552 ± 7 Ma that lasted up to 50 Ma after CAI as residual melts could have been retained in the mantle of Vesta. Younger ages for basaltic eucrites have also been obtained using the bulk rock ^{182}Hf-^{182}W isotopic system, with a crystallization age for Camel Donga of 22–23 Ma after CAI (Kleine et al., 2005; Touboul et al., 2015), as well as for zircon ^{182}Hf-^{182}W ranging from 2.3 ± 1.5 to 35^{+11}_{-6} Ma after CAI (Roszjar et al., 2016). The reason of this discrepancy is not clear, and only one sample (Camel Donga) has been replicated in each of those studies and the present one. Camel Donga is known for showing important shock features (Zhou et al., 2013). Srinivasan et al. (2007) also obtained older ^{182}Hf-^{182}W ages for what they interpreted as being magmatic zircons, <6.8 Ma after the core segregation on Vesta. Except the study of Srinivasan et al. (2007), it should be noted that both ^{182}Hf-^{182}W whole rock and zircon ages are systematically younger than ^{26}Al-^{26}Mg and ^{53}Mn-^{53}Cr ages for the HED groups (see compilation in Zhou et al., 2013 and references therein), even though zircon ages are difficult to reset and are interpreted as true magmatic ages (Srinivasan et al., 2007; Zhou et al., 2013; Roszjar et al., 2016). However, Iizuka et al. (2015) interpreted their U-Pb ages on zircons from the Agoult basaltic eucrite at 4554.5 ± 2.0 Ma (i.e. ~13 Ma after CAI based on the absolute Pb-Pb age of

the Efremovka 22E CAI (Connelly et al., 2012) used as anchor in this study) as representing a large metamorphic event on Vesta. One possible explanation could be the higher sensitivity to thermal metamorphic resetting and/or to terrestrial contamination of the ^{182}Hf-^{182}W systematic compared to the ^{26}Al-^{26}Mg systematic (Kleine et al., 2005, 2009; Touboul et al., 2015), but the reason for younger zircon ages is not clear.

4.2.2. Metamorphism in basaltic eucrites

The third basaltic eucrite (Y-792510) has an internal ^{26}Al-^{26}Mg isochron relative age of $6.75^{+2.15}_{-0.66}$, i.e. 2 Ma younger than the WR isochron obtained on all basaltic eucrites ($2.66^{+1.39}_{-0.58}$ Ma after CAI, Y-792510 included), and also a higher $\delta^{26}Mg^{*}_{0}$ value than the 2 other basaltic eucrites (0.036 ± 0.005, compared to -0.001 ± 0.030 and 0.012 ± 0.006). The younger age obtained on Y-792510 could actually reflect resetting of ^{26}Al-^{26}Mg systematics by secondary processes such as a metamorphic event. Previous studies have shown that basaltic eucrites (Takeda and Graham, 1991; Yamaguchi et al., 1996, 1997, 2009) and more recently diogenites (Yamaguchi et al., 2011) are often metamorphosed. While almost all eucrites have been metamorphosed to some degree, the extent of metamorphism varies. Takeda and Graham (1991) developed a classification based on the pyroxene mineralogy and texture that defines six different types of metamorphosed eucrite, with the type 1–6 representing progressive degree of higher metamorphism. Later, a type 7 was also defined by Yamaguchi et al. (1996), that shares some characteristics of type 4 (Ca-zoning in pyroxenes) and of type 6 (pyroxenes partly inverted pigeonite). Yamato-792510 is known as a highly metamorphosed eucrite of type 6 (Takeda and Graham, 1991), with younger ^{87}Rb-^{87}Sr and ^{147}Sm-^{143}Nd ages (Nyquist et al., 1997). The younger ^{26}Al-^{26}Mg internal age compared to the two other basaltic eucrites in this study is thus consistent with metamorphic resetting that occurred after its initial crystallization but still during the lifetime of ^{26}Al, as this sample can still be dated. Internal isochrons of mineral separates indicate the age of crystallization or later resetting, e.g. by metamorphism, while WR (external) isochrons provide only the crystallization age if samples are co-genetic. From our data the WR age for basaltic eucrites ($2.66^{+1.39}_{-0.58}$ Ma after CAI) corresponds within error to the average crystallization age obtained for Camel Donga and Y-793591 (Fig. 3a and b), while the internal age of Y-792510 is significantly younger (Table 3; Fig. 3c). In addition, the fact that the $\delta^{26}Mg^{*}_{0}$ is higher for Y-792510 (0.036 ± 0.005) compared to the 2 other basaltic eucrites (-0.001 ± 0.030 and 0.012 ± 0.006) also indicates that the isochron was shifted. This supports our hypothesis that the mineral separate ages obtained for Camel Donga and Y-793591 reveal their crystallization age, while the younger age obtained for Y-792510 reflects resetting when ^{26}Al was still extant, probably due to an impact metamorphic event which is supported by petrographic evidence. The case of Y-792510 shows that WR and mineral separate isochrons are clearly complementary by providing different information.

The younger ages observed here for the three cumulate eucrites could similarly be interpreted as resetting ages induced by impact metamorphism. However, impact metamorphism is not obvious in the samples measured here, and the texture and composition of cumulate eucrites are more consistent with formation by slow cooling within the eucrite crust (Yamaguchi et al., 1996, 1997). In addition, their initial $\delta^{26}Mg^{*}_{0}$ is also similar to the one of basaltic eucrites within error. Based on these observations, we thus suggest that the internal isochrons obtained for cumulate eucrites truly represented their crystallization ages of these samples.

4.2.3. Young ^{26}Al-^{26}Mg ages of diogenites

Diogenites studied here, despite having a non-chondritic ^{27}Al-^{24}Mg ratio, have no anomaly in $\delta^{26}Mg^{*}$ that would normally be expected if these objects were formed while ^{26}Al was extant. This result is consistent with data from Bizzarro et al. (2005) and Schiller et al. (2010a), even though Schiller et al. (2011) suggested some diogenites could have a small $\delta^{26}Mg^{*}$ anomaly. On the other hand, diogenites seem to plot on the HED WR isochron (Fig. 2a), as also observed for WR ^{53}Mn-^{53}Cr HED isochron (Trinquier et al., 2008; Day et al., 2012). The first feature can only be explained if these meteorites were formed after the complete extinction of ^{26}Al while the second implies the presence of ^{26}Al when diogenite crystallized. When looking to diogenite external or internal isochrons, no meaningful age can be obtained (Fig. 4). A simple explanation would be that, as for the basaltic eucrite Y-792510, diogenites have suffered impact metamorphism and have thus been reset, but after the complete extinction of ^{26}Al in this case. However, such an event would be consistent with younger (or no) internal isochrons, but not with younger WR age as deduced from the lack of $\delta^{26}Mg^{*}$ anomaly. On the other hand, with diogenites being almost monomineralic (orthopyroxene), one could argue that the small spread observed between diogenites prevents obtaining meaningful isochrons within analytical uncertainty. When looking at the spread between the different fractions, diogenites indeed show systematically a small spread in ^{27}Al/^{24}Mg, between 0.026 and 0.031, i.e. a ratio of ~0.8 for WR, and a ratio of ~3 for the two internal isochrons. Such a small ratio is also observed for the WR basaltic eucrite isochron (~1.6) and Camel Donga internal isochron (~2.0) that both give resolvable ages. Taking the full range displayed by diogenites, and assuming they all crystallized at the same time without any resetting, no meaningful isochron is obtained (not shown). Finally, it is even more difficult to erase a bulk rock $^{26}Mg^{*}$ anomaly by an impact resetting as this would imply open system metamorphism by fluid circulation. It was suggested that some impacts may have brought fluids on Vesta (Warren et al., 2014) but such an aqueous alteration is not seen in diogenites. Instead, the combination of no $^{26}Mg^{*}$ anomaly despite non-chondritic ^{27}Al/^{24}Mg and the absence of both external and internal isochron better suggests that diogenites were formed after the complete extinction of ^{26}Al. This implies that diogenites are younger than 7.25 Ma after CAI, corresponding to the youngest resolvable relative age obtained on

cumulate eucrite in this study. This also implies that the presence of diogenites close from the basaltic eucrite isochron is fortuitous. It is consistent with the observation of an errorchron with all HED but an isochron with eucrites.

By using model isochrons, Schiller et al. (2011) proposed that variation of $\delta^{26}Mg^*$ could suggest the formation of diogenites during the first 2.5 Ma after CAI formation, hence being older than eucrites. They interpreted this as diogenites and eucrites being respectively the early and late magmas from a single crystallizing magma ocean, thus being co-magmatic as proposed by other studies (e.g. Fowler et al., 1995; Schiller et al., 2017). Interpreting age data for diogenites is clearly not a simple task but it should be noted that two samples replicated in the present study (Bilanga and Tatahouine) are consistent with values from Bizzarro et al. (2005) and Schiller et al. (2010a), but not with the Schiller et al. (2011) study. In addition, the hypothesis of diogenites being early products of a vestan magma ocean cannot be reconciled with their refractory incompatible lithophile element content (Mittlefehldt, 2015). Finally, as explained in the present study, we do not reach the same conclusion that eucrites and diogenites share a common source. If indeed diogenites are younger than eucrites, this means that great caution should be taken when constructing and interpreting planetary isochrons calculated using both diogenites and eucrites.

To be consistent with our study, formation of diogenites thus requires either protracted magmatic activity, or a second period of magmatic activity on Vesta (Barrat et al., 2010; Yamaguchi et al., 2011). Barrat et al. (2008) and Barrat (2004) argued that one mechanism to explain this diogenitic magmatism is through the re-melting of magma ocean cumulates. The heat source for a re-melting event is unclear as, at that time, ^{26}Al was completely extinct as suggested here. One possibility is that a mantle overturn could induce re-melting. Normally, a mantle overturn would happen only when a body is entirely crystallized with denser Fe-rich cumulate at the top of the mantle (Elkins-Tanton et al., 2003), but because of the smaller gravity of Vesta and a higher heat flux, it is possible that a mantle overturn occurred within Vesta with a partially solid mantle overlaid by a mush portion (Elkins-Tanton et al., 2008). Because Vesta is a much smaller body compared to previous studies on Mars (Elkins-Tanton et al., 2003), in this case, a higher density of the upper cumulates could be reached by colder temperature and higher proportion of minerals at the top of the magma ocean (Elkins-Tanton et al., 2008). Another possibility to explain this delayed diogenite magmatism could be related to trapped melt remaining for several tens of millions of year in the vestan mantle (Zhou et al., 2013). However, in this case, it is still unclear what could trigger the emplacement of diogenites. It should be noted that some diogenites may have intruded the eucritic crust and subsequently crystallized earlier compared to what is proposed here, as some diogenites show a negative $\delta^{26}Mg^*$ (Schiller et al., 2011). On the contrary, the positive anomalies found by Schiller et al. (2011) in some other diogenites cannot be reconciled with their subchondritic $^{27}Al/^{24}Mg$ and our preferred interpretation would be that they have been contaminated by the eucritic crust, as evidenced by their bulk composition (e.g. Mittlefehldt, 2015). As such, the chemical trend observed by Schiller et al. (2011) could represent a mixing trend.

4.3. Differentiation of Vesta

Evidence that Vesta is the parent body of HED is generally well accepted, especially since the Dawn mission that clearly identified Vesta as the parent body of HED meteorites (McSween et al., 2013). Previous studies based on ^{182}Hf-^{182}W systematic (Quitté et al., 2000; Kleine et al., 2005, 2009; Touboul et al., 2015) have shown that Vesta underwent global melting and core-mantle segregation. It is usually considered that the heat provided by ^{26}Al and possibly ^{60}Fe decay was enough to entirely melt planets and large asteroids to form a magma ocean (Elkins-Tanton et al., 2003). This hypothesis is corroborated by the O-isotope homogeneity in the HED, that could only be induced by the existence of magma ocean on Vesta (Greenwood et al., 2014). Even though Wasson (2013) argued that neither ^{26}Al decay or giant impact would have delivered sufficient energy to produce a magma ocean on Vesta, some thermal models (Ghosh and McSween, 1998; Sahijpal et al., 2007; Neumann et al., 2014) do suggest that the decay of ^{26}Al and ^{60}Fe could have provided the heat source to form a shallow or global magma ocean on Vesta. Recently, analyzes of siderophile abundances in eucrites and diogenites have indicated that Vesta could have been completely molten during its core formation (Steenstra et al., 2016).

Even though basaltic eucrites, cumulate eucrites and diogenites did not crystallize at the same time, they could still share a common source (e.g. Mandler and Elkins-Tanton, 2013; Schiller et al., 2017). This can be tested by modeling when eucrites and diogenites diverged from a chondritic evolution, and this model age could then be interpreted as the differentiation age of Vesta, likely related to a magma ocean stage. Calculating these model ages require us to make some assumptions about the evolution of Vesta, namely, that Vesta started from a chondritic precursor, followed by differentiation of the source and formation of magma at the surface of the asteroid. A model age is then obtained by combining the chondritic average value and the whole rock measurements of our samples (Bizzarro et al., 2005; Baker et al., 2012). The chondritic average value used here corresponds to non-CAI-bearing chondrites with a $\delta^{26}Mg^*$ present-day value of -0.0015 ± 0.0013 (Schiller et al., 2010b; Baker et al., 2012). The model HED isochron gives an initial $(^{26}Al/^{27}Al)_0$ ratio of $3.34 \pm 0.87 \times 10^{-6}$ that can be translated to a single model relative age of $2.90^{+0.31}_{-0.24}$ Ma after CAI (Fig. 7a) for all the HED samples. Considering the previous discussions about the implication of building planetary isochrons, model isochrons have also been prepared for each group of HED. These model WR isochrons give an initial $(^{26}Al/^{27}Al)_0$ ratios of $3.32 \pm 0.47 \times 10^{-6}$ for basaltic eucrites (Fig. 7b) and $3.80 \pm 3.21 \times 10^{-6}$ for cumulate eucrites (Fig. 7c). By using the same anchor value previously used in this study,

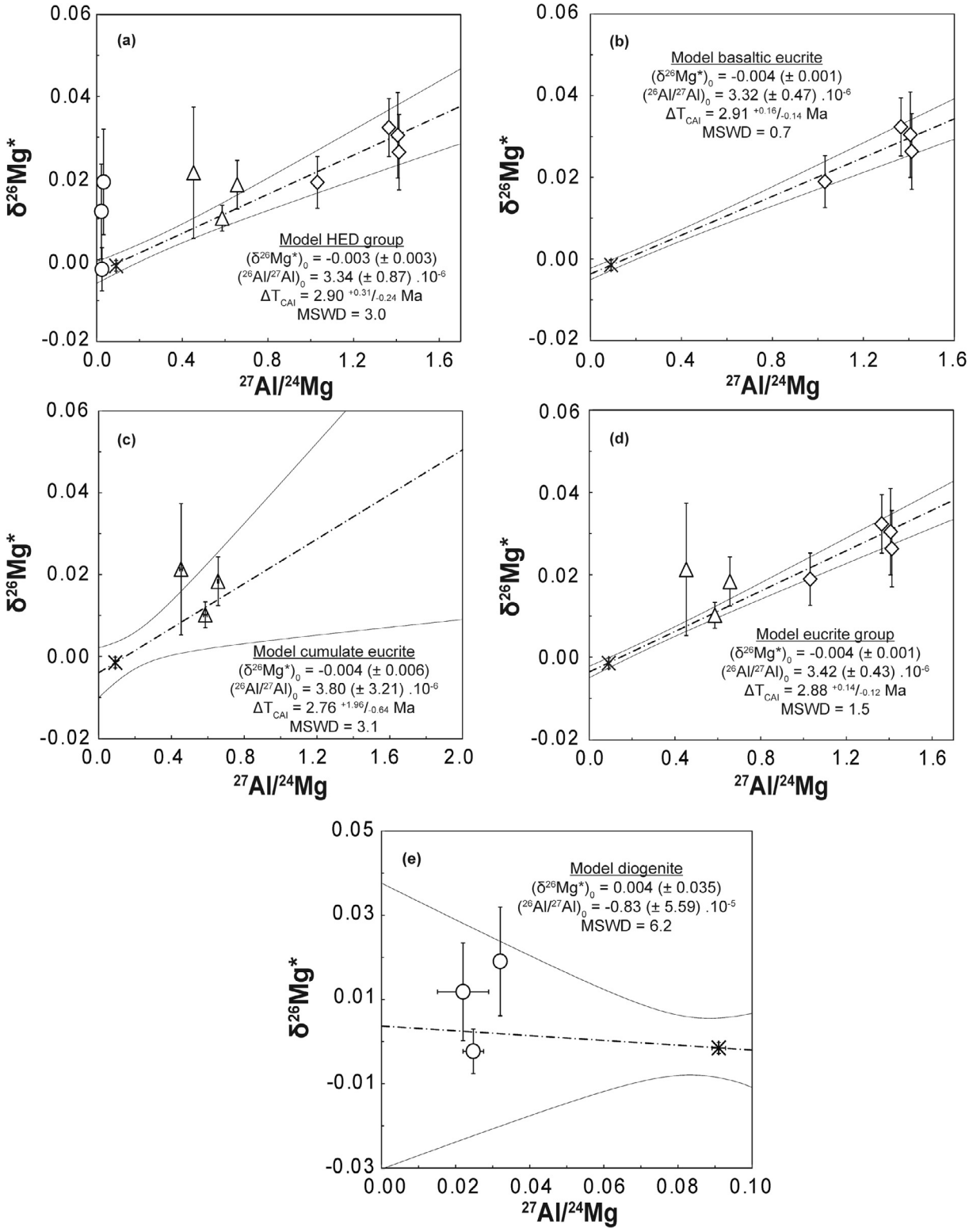

Fig. 7. Whole rock model regressions for (a) HED group ($n = 11$, errorchron in the 95% confidence interval); (b) basaltic eucrites ($n = 5$, isochron in the 95% confidence interval) and (c) cumulate eucrites ($n = 4$, isochron in the 95% confidence interval); (d) all eucrites ($n = 8$, isochron in the 95% confidence interval); (e) diogenites ($n = 4$, errochron and non-resolvable $(^{26}Al/^{27}Al)_0$). The star symbol represents the chondritic value (Schiller et al., 2010b). Calculations made using the Isoplot software (Ludwig, 2012). The solid lines are the 2σ error envelop.

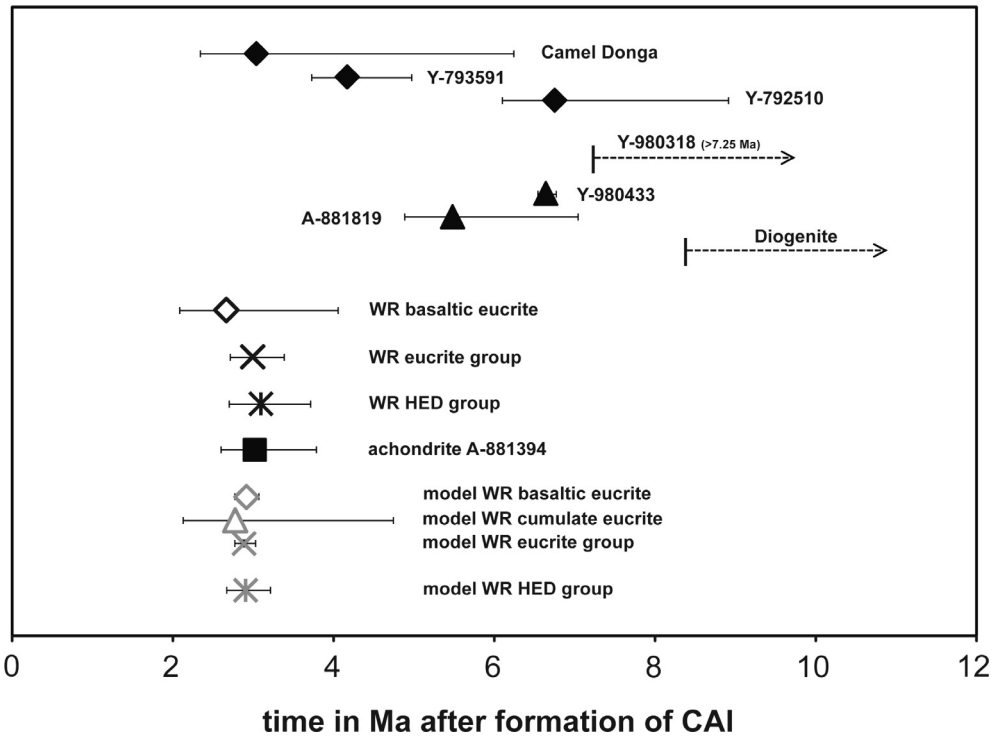

Fig. 8. Summary of the different relative ages obtained for the eucrite and diogenite samples analyzed in this study, calculated with the $(^{26}Al/^{27}Al)_0$ ratios of Efremovka CAI 22E (Larsen et al., 2011) anchor value. Diamonds are for basaltic eucrites, triangles for cumulate eucrites and square for A-881394 achondrite. The black symbols correspond to ages obtained with internal isochrons constructed on mineral fractions and the filled grey triangle is the non-resolvable age for Y-980318. The white symbols are the WR age obtained with WR isochron. The grey symbols correspond to the model ages obtained with WR model isochrons. Error bars are 2σ.

the $(^{26}Al/^{27}Al)_0$ ratio can be translated to a model relative age of $2.91^{+0.16}_{-0.14}$ Ma after CAI for basaltic eucrites (Fig. 7b) and $2.77^{+1.96}_{-0.64}$ Ma after CAI for cumulate eucrites (Fig. 7c). For diogenites, a model age cannot be obtained as they contain no correlated excess or deficit in ^{26}Mg with $^{27}Al/^{24}Mg$ ratio (Fig. 7e). As already observed for external isochrons, the robustness of the model isochron expressed by the MSWD value is much better when diogenites are not considered with basaltic eucrites model isochron (errorchron with MSWD of 3.0 for all HED compared to isochron with MSDW of 0.7 for basaltic eucrites only). All these model ages obtained are presented in Table 3.

Previous studies support the hypothesis of a common eucrite source (Mittlefehldt, 1994; Treiman, 1997; Barrat et al., 2000, 2010; Mittlefehldt, 2015), also confirmed recently by $\varepsilon^{182}W$ and $^{182}Hf/^{180}Hf$ (Touboul et al., 2015). If we assume that basaltic and cumulate eucrites are comagmatic from a source that differentiated in a single event then we can calculate a single model age for all eucrites. By combining all eucrites, a model age of $2.88^{+0.14}_{-0.12}$ Ma after CAI is obtained for a eucrite source. If we combine our data with previous WR $\delta^{26}Mg^*$ analyses from Bizzarro et al. (2005) and Schiller et al. (2010a), we also obtain a similar result corresponding to an initial model $(^{26}Al/^{27}Al)_0$ ratio of $2.58 \pm 0.43 \times 10^{-6}$ and a relative age of $3.17^{+0.16}_{-0.19}$ Ma after CAI.

The absence of model WR regression for diogenites is actually consistent with the suggestion that even if the source of diogenites differentiated from a chondritic reservoir, their actual chemical signature do not reflect a simple two-stage evolution. It has indeed been proposed that their composition has been altered due to contamination by various amount of trapped melt in magma chambers (Mittlefehldt, 1994; Fowler et al., 1995; Barrat et al., 2010). As such, it is impossible to know if they were cogenetic with basaltic eucrites or not. The fact that diogenites plot on the HED model isochron seems again fortuitous, as deduced for the WR HED isochron (see point 2.3). Another explanation to the absence of model WR isochron could be that diogenites record a multi-stage differentiation of Vesta, but the contamination of diogenites by the already formed eucrite crust is strongly supported by the incompatible trace element composition (Barrat et al., 2010). This scenario requires that diogenites are younger than eucrites, in agreement with the present discussion (Section 4.2.3).

The model age obtained with all eucrites indicate that the differentiation of Vesta occurred $2.88^{+0.14}_{-0.12}$ Ma after the formation of CAI's, i.e. at the same time within error compared to the establishment of the eucritic crust. At this time, following the results obtained in the present study, Vesta probably experienced global melting with the formation

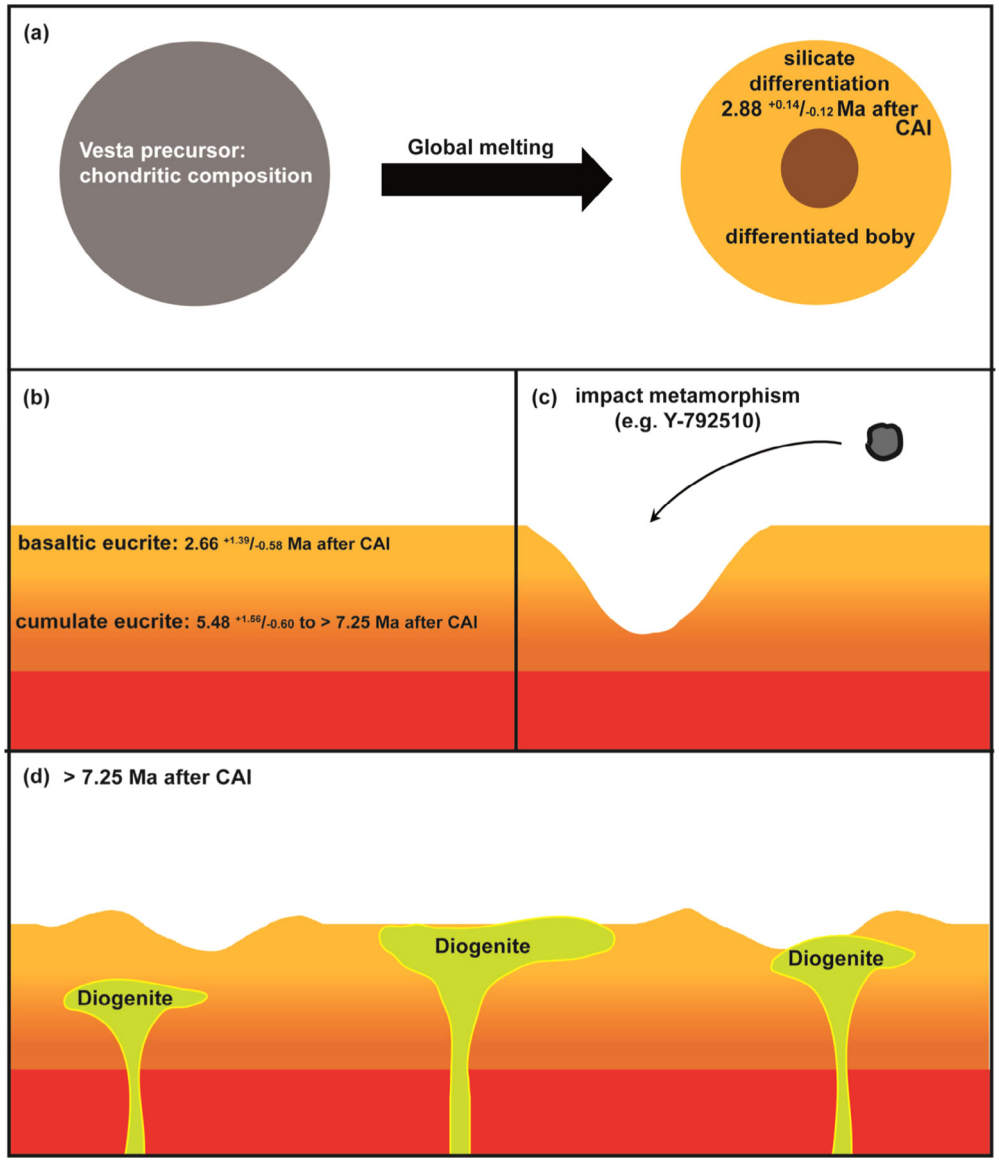

Fig. 9. summary of the geological history of Vesta, where (a) represents the differentiation of Vesta and the formation of a differentiated reservoir being the source of all eucrites from a chondritic precursor; (b) represents the eucrite crust formation with a short magmatic activity (~2 Ma) that formed the basaltic eucrites, followed by the slow cooling of cumulate eucrites deeper in the crust; (c) eucrites evidence impact metamorphism at the surface of Vesta during the lifetime of ^{26}Al suggested by the young internal age of the Y-792510 basaltic eucrite (d) represents the formation of diogenites in intrusions or extrusions during a second magmatic activity.

of a magma ocean and the differentiation of the eucrite source from a chondritic reservoir. Core formation age deduced by the ^{182}Hf-^{182}W isotopic system suggesting formation at 4 ± 2.2 Ma (Kleine et al., 2004) and by the ^{60}Fe-^{60}Ni isotopic system at $3.7^{+2.5}_{-1.7}$ Ma after CAI formation (Tang and Dauphas, 2012). Core formation is supposed to occur contemporaneously with the establishment of the magma ocean and those results are thus coherent with our proposed age for the setting of a magma ocean on Vesta. On the other hand, Touboul et al. (2015) recently suggested that core formation likely occurred within ~1 Ma after CAI formation. Such an early timing would imply that Vesta remained completely molten for ~2 Ma to be consistent with the differentiation age obtained here. As summarized in Fig. 8, the eucrite model age is similar within error with the crystallization age of basaltic eucrites. This implies that the eucritic magmatism was directly related to the formation and crystallization of a magma ocean on Vesta, with concomitant extrusion of lava flows at the surface of the asteroid. Despite cumulate eucrites may share the same source as basaltic eucrites, there is a resolvable gap between the global differentiation of Vesta and their crystallization, reinforcing their position deep in the crust of Vesta.

Table 4
Different ages obtained for A-881394 anomalous achondrite with different short-lived and long-lived isotopic systems.

Isotopic system	$\Delta t_{CAI} \pm 2\sigma$ (Ma)	$T_a \pm 2\sigma$ (Ma)	Ref.
^{26}Al-^{26}Mg	$3.02^{+0.76}_{-0.43}$	$4564.33^{+0.71}_{-1.04}$	This study
	$3.39^{+0.18}_{-0.22}$	$4563.96^{+0.46}_{-0.50}$	Srinivasan (2002)
	$3.99^{+0.25}_{-0.33}$	$4563.36^{+0.53}_{-0.61}$	Nyquist et al. (2003)
	$3.91^{+0.05}_{-0.06}$	$4563.44^{+0.33}_{-0.34}$	Wadhwa et al. (2009)
	$3.75^{+0.08}_{-0.09}$	$4563.60^{+0.36}_{-0.09}$	Wimpenny et al. (2013)
^{53}Mn-^{53}Cr		4565.24 ± 0.46	Nyquist et al. (2003)
		4564.29 ± 0.28	Wadhwa et al. (2009)
Pb-Pb		4566.5 ± 0.2	Wadhwa et al. (2009)
		4565.57 ± 0.55	Koefoed et al. (2015)

All Δt_{CAI} and absolute ages have been recalculated from literature (^{26}Al/^{27}Al)$_0$ using the Efremovka 22E CAI (Larsen et al., 2011; Connelly et al., 2012) as anchor value.

4.4. Formation of the crust of Vesta

Our new ^{26}Al-^{26}Mg data for diogenites, basaltic and cumulate eucrites can help constraining the differentiation of Vesta and the formation of its complex crust. Considering a chondritic precursor for Vesta, we can interpret the magmatic evolution of Vesta into several steps. The first step is the formation of the Solar System represented by the age of CAI condensation and the accretion of the parent body that cannot be dated in the present study. The second step corresponds to the establishment of a magma ocean on Vesta from a chondritic precursor and is represented by the model WR isochron age of eucrites $2.88^{+0.14}_{-0.12}$ Ma after CAI formation (Fig. 9a). This step also corresponds to the formation of the core. The third step involves the formation of the crust of Vesta. While the magma ocean was established and started to crystallize, a first episode of magmatic activity occurred contemporaneously that produced the upper part of Vesta crust, composed mainly of basaltic eucrites. The crystallization ages represented by ^{26}Al-^{26}Mg WR basaltic eucrite isochron suggest that this magmatic activity took place at $2.66^{+1.39}_{-0.58}$ Ma after CAI, in agreement with Quitté and Birck (2004) who suggested that the formation of basaltic liquid followed the differentiation of Vesta by 0.6 Ma (Fig. 9b). Deeper in the crust, cumulate eucrites could have been formed either by a later pulse of intrusive magmatic activity or by slow cooling in depth from a single magmatic event, but in any case from a common source to all eucrites. The crystallization age obtained with the ^{26}Al-^{26}Mg isotopic system suggests a closure time between $5.48^{+1.56}_{-0.60}$ to >7.25 Ma after CAI (Fig. 9b) for the three cumulate eucrites analyzed in this study. The crystallization of cumulate eucrites ranged over a longer time period compared to basaltic eucrites, in agreement with their location deeper in the crust of Vesta. The younger age obtained for the basaltic eucrite Y-792510 suggests that large impacts could have occurred very early in the Solar System history when ^{26}Al was still extant (Fig. 9c). Impact metamorphism seems a very important process in the history of Vesta crust and could easily explain the large range of age obtained for basaltic and cumulate eucrites using different isotope systems. Finally, the formation of diogenites seems younger and more complex compared to eucrites, and could be related to a late intrusive magmatic activity peak after the complete extinction of the ^{26}Al and possible contamination by the eucrite crust (Barrat et al., 2008, 2010) (Fig. 9c). Yamaguchi et al. (2011) suggested that the diogenites melt were produced by the re-melting of magma ocean cumulate and intruded the eucrite crust. The cause of this re-melting is not constrained until now, but could be related to a mantle overturn.

4.5. The case of A-881394 achondrite

The internal isochron constructed on mineral separates obtained for A-881394 unique achondrite gives a relative crystallization age of $3.02^{+0.76}_{-0.43}$ Ma after CAI. For comparing this age with literature data, we recalculated the different existing ^{26}Al-^{26}Mg ages from the initial (^{26}Al/^{27}Al)$_0$ ratios found in the literature with the same anchor values used in this study. Some differences can be observed when recalculating ages from literature (Table 4). Our A-881394 age is systematically older compared to other ^{26}Al-^{26}Mg studies. However, it compares well within error with the ^{53}Mn-^{53}Cr ages while it is slightly younger than Pb-Pb ages. The age discrepancy for ^{26}Al-^{26}Mg could potentially be related to localized disturbance and resetting following impact metamorphism. Even though both Al and Mg are considered as relatively robust to diffusion (LaTourrette and Wasserburg, 1998), plagioclase is a phase that can be prone to diffusive Mg loss (Van Orman et al., 2014). The good concordance of the ^{26}Al-^{26}Mg age obtained here with another short-lived system, and the fact that this age is one of the older among Al-Mg published age for A-881394 both suggest that the subsample used has been relatively well-preserved from impact resetting.

Even though A-881394 was considered at first as a cumulate eucrite, the age discrepancy between this sample and the cumulate eucrites for their crystallization ages is difficult to reconcile. On the other hand, the crystallization age of A-881394 is very similar to the one obtained for basaltic eucrites in the present study. However, the absence

of meaningful correlation with WR basaltic eucrites indicates that A-881394 is not co-genetic with basaltic eucrites. Accordingly, differences in O, Ti and Cr isotope ratios clearly suggest that A-881394 achondrite is derived from another parent body (Scott et al., 2009; Greenwood et al., 2014; Sanborn and Yin, 2014; Williams et al., 2015). When constructing a model age isochron with all eucrites and A-881394, we obtain a resolvable correlation implying that we cannot rule out the fact that A-881394 is related to a parent body that was chondritic and differentiated at the same time than Vesta. It should also be noted that a regression with all WR HED (both types of eucrites and diogenites) and WR A-881394 yields a correlation with a meaningful ($^{26}Al/^{27}Al)_0$ ratio of $3.48 \pm 1.19 \times 10^{-6}$ but a poor MSWD of 5.9 (not shown). This mathematically correct but geologically absurd result stresses one more time that the interpretation of planetary isochrons should be done with caution. On the other hand, similar model isochrons between basaltic eucrites and A-881394 indicates that the melting and differentiation of chondritic silicate bodies very early at the beginning of the Solar System was certainly a widespread phenomenon.

5. CONCLUSION

The study of ^{26}Al-^{26}Mg systematic on HED meteorites showed that internal isochrons are required to evaluate the geological meaning of planetary isochrons. Even though all HED seem to plot on a unique isochron, the crystallization ages obtained for cumulate eucrites and diogenites are resolvably younger compared to basaltic eucrites. As such, the ^{26}Al-^{26}Mg ages obtained both on whole-rock and mineral separates for eucrite and diogenite samples allow us to refine the geological history of Vesta:

1. Internal ^{26}Al-^{26}Mg data indicate that there is a gap between the crystallization ages of basaltic ($2.66^{+1.39}_{-0.58}$ Ma after CAI) and cumulate ($5.48^{+1.56}_{-0.60}$ to >7.25 Ma after CAI) eucrites. This implies that the eucrite crust was formed in two steps. The first step corresponds to the formation of the upper part of the crust by basaltic eucrites during a short (~2 Ma) extrusive magmatic activity. The second step consists of the crystallization of the cumulate eucrite by slow cooling deeper in the crust.
2. While basaltic and cumulate eucrites crystallized at distinctly different times, model ages constructed on all eucrites seem to indicate that they could share a common source that differentiated from a chondritic precursor at $2.88^{+0.14}_{-0.12}$ Ma after CAI. This time range overlaps with the crystallization ages of basaltic eucrite.
3. Since no anomaly in $\delta^{26}Mg^*$ has been found in diogenites despite them showing a subchondritic Al/Mg ratio, and because no external or internal isochrons could have been obtained, we suggest that diogenites are younger than eucrites and formed after the complete extinction of ^{26}Al. Consequently, they cannot precisely be dated by ^{26}Al-^{26}Mg isotopic system. The impossibility of also obtaining model age indicates a history more complex than simple differentiation from a chondritic precursor. This complexity could be explained if these meteorites formed by intrusions in the eucrite crust during a second magmatic activity that took place after the complete extinction of ^{26}Al, and with possible crustal contamination. Mantle overturn could be a mechanism to explain the protracted magmatic activity on Vesta.
4. A younger crystallization age obtained for the Y-792510 basaltic eucrite suggests that the basaltic crust had experienced impact metamorphism of sufficient magnitude to reset the ^{26}Al-^{26}Mg isotopic system very early in the Solar System history, while ^{26}Al was still extant.
5. Finally, internal ^{26}Al-^{26}Mg isochron obtained for A-881394 achondrite indicates that this sample is related to a parent body that was initially very similar to Vesta (i.e. chondritic) and differentiated contemporaneously.

ACKNOWLEDGMENTS

GH and VD thank Wendy Debouge for technical support in the clean lab, and Jeroen de Jong for the technical and analytical support on the Nu-plasma I and II at ULB. The help of Nadine Mattielli and Nu Instrument Ltd has also been greatly appreciated. We thank the National Institute of Polar Research and the Royal Belgian Institute of Natural Sciences for providing meteorite samples. VD thanks Francis Albarède and Ghylaine Quitté for insightful discussions on isochrons. GH thanks the FRIA-FNRS and the IUAP "Planet Topers" for financial support. VD thanks the FRS-FNRS and the ERC StG 336718 "ISoSyC" for financial support. QZY acknowledges NASA grants NNX14AM62G and NNX16AD34G. The AE Dimitri Papanastassiou, 2 anonymous reviewers and Jean-Alix Barrat are thanked to their constructive comments and suggestions.

APPENDIX A

See Table A1.

Table A1
Compilations of all Al-Mg data obtained in the present study.

Sample	$^{27}Al/^{24}Mg$	2 se	$\delta^{26}Mg^*$	2 se	n	$\delta^{26}Mg^*$	2 se	n	$\delta^{26}Mg^*$	2 se	n	$\delta^{26}Mg^*$	2 se	n
			ULB (Nu-plasma I)			ULB (Nu-plasma II)			UCDavis (Neptune)			All data combined		
Basaltic eucrites														
Millbillillie WR	1.407	0.008	0.027	0.031	3				0.032	0.010	8	0.030	0.010	11
Camel Donga WR	1.412	0.018	0.020	0.014	4				0.030	0.012	7	0.026	0.009	11
px.	0.995	0.013	0.018	0.031	5				0.025	0.014	8	0.022	0.014	13
px-pl.	1.798	0.028	0.038	0.015	5				0.038	0.012	8	0.038	0.009	13
Y-792510 WR	1.365	0.019	0.029	0.009	17				0.042	0.007	6	0.032	0.007	23
px. 1	0.105	0.008	0.036	0.015	3				0.038	0.011	5	0.037	0.008	8
px. 2	0.146	0.025	0.068	0.020	4				0.038	0.011	10	0.046	0.012	14
pl.	42.567	2.220				0.064	0.023	2				0.064	0.023	2
Y-793591 WR	1.031	0.019	0.023	0.008	6				0.014	0.009	5	0.019	0.006	11
px. 1	0.240	0.018	0.013	0.007	4				0.016	0.010	6	0.015	0.006	10
px. 2	0.555	0.032	0.019	0.028	4							0.019	0.028	4
px-pl.	1.924	0.015	0.026	0.006	3				0.027	0.003	5	0.026	0.003	8
Cumulate eucrites														
Y-980318 WR	0.586	0.010	0.009	0.008	1				0.010	0.004	7	0.010	0.003	8
px. 1	0.027	0.001	−0.004	0.012	19							−0.004	0.012	19
px. 2	0.190	0.006	0.001	0.013	11							0.001	0.013	11
pl.	92.823	1.690				0.022	0.005	3				0.022	0.005	3
Y-980433 WR	0.453	0.008	0.026	0.023	8				0.012	0.016	4	0.021	0.016	12
px. 1	0.040	0.003	0.020	0.005	3				0.020	0.008	5	0.020	0.005	8
px. 2	0.143	0.005	0.016	0.013	18				0.011	0.012	7	0.015	0.010	25
pl.	95.064	0.981				0.084	0.006	3				0.084	0.006	3
A-881819 WR	0.657	0.004	0.030	0.012	1				0.017	0.005	8	0.018	0.006	9
Fr 1 (heavy px.)	0.279	0.004	−0.006	0.046	3	0.040	0.036	5				0.022	0.031	8
Fr 2 (< 0.45 A)	0.709	0.022				0.040	0.018	4				0.040	0.018	4
Fr 3 (0.45 to 0.65 A)	0.939	0.007	0.024	0.030	7	0.049	0.011	4				0.033	0.020	11
Fr 4 (0.65 to 0.75 A)	1.775	0.024				0.052	0.031	3				0.052	0.031	3
Fr 5 (0.75 to 1.1 A)	2.884	0.027	0.019	0.018	3	0.047	0.028	5				0.036	0.018	8
Fr 6 (> 1.1 A)	9.495	0.199				0.039	0.013	7				0.039	0.013	7
Diogenites														
Bilanga WR	0.025	0.003	−0.002	0.005	9							−0.002	0.005	9
Fr 1 (HD,<0.45 A)	0.027	0.005	0.006	0.007	4							−0.020	0.007	4
Fr 2 (HD, 0.45 to 0.50 A)	0.026	0.003	0.002	0.017	13							−0.030	0.017	13
Fr 3 (HD, > 0.50 A)	0.036	0.004	0.004	0.021	13							0.001	0.021	13
Fr 4 (LD, < 0.45 A)	0.020	0.002	−0.013	0.031	7							−0.013	0.031	7
Fr 5 (LD, 0.45 to 0.50 A)	0.022	0.002	0.008	0.006	5							0.008	0.006	5
Fr 6 (LD, > 0.50 A)	0.058	0.004	0.007	0.014	6							0.007	0.014	6

(*continued on next page*)

Table A1 (*continued*)

Sample	$^{27}Al/^{24}Mg$	2 se	$\delta^{26}Mg^*$	2 se	n	$\delta^{26}Mg^*$	2 se	n	$\delta^{26}Mg^*$	2 se	n	$\delta^{26}Mg^*$	2 se	n
			ULB (Nu-plasma I)			ULB (Nu-plasma II)			UCDavis (Neptune)			All data combined		
Johnstown WR	0.032	0.002	0.019	0.013	10							0.019	0.013	10
Fr 1 (HD, < 0.40 A)	0.052	0.008	0.019	0.009	7							0.019	0.009	7
Fr 2 (HD, 0.40 to 0.45 A)	0.035	0.003	0.044	0.013	2							0.044	0.013	2
Fr 3 (HD, > 0.45 A)	0.039	0.002	0.019	0.031	5							0.019	0.031	5
Fr 4 (LD, < 0.45 A)	0.063	0.006	0.008	0.034	6							0.008	0.034	6
Fr 5 (LD, 0.45 to 0.50 A)	0.035	0.002	0.023	0.003	3							0.023	0.003	3
Fr 6 (LD, > 0.50 A)	0.114	0.010	0.000	0.013	11							0.000	0.013	11
Tatahouine WR	0.022	0.007	0.012	0.012	9							0.012	0.012	9
Fr 1 (HD, < 0.30 A)	0.084	0.004	−0.035	0.001	2							−0.035	0.001	2
Fr 2 (HD, 0.30 to 0.40 A)	0.067	0.004	−0.025	0.022	4							−0.025	0.022	4
Fr 3 (HD, 0.40 to 0.45 A)	0.060	0.008	−0.016	0.046	5							−0.016	0.046	5
Fr 4 (HD, > 0.45 A)	0.058	0.033	0.011	0.013	4							0.011	0.013	4
Fr 5 (LD, < 0.30 A)	0.056	0.021	0.019	0.004	3							0.019	0.004	3
Fr 6 (LD, 0.30 to 0.40 A)	0.022	0.002	−0.030	0.003	2							−0.030	0.003	2
Fr 7 (LD, 0.40 to 0.45 A)	0.020	0.001	−0.022	0.011	3							−0.022	0.011	3
Fr 8 (LD, > 0.45 A)	0.043	0.003	0.021	0.035	5							0.021	0.035	5
A-881394 achondrite														
A-881394 WR	0.932	0.007				0.076	0.020	6				0.076	0.020	6
px. 1	0.060	0.000				0.074	0.015	6				0.074	0.015	6
px. 2	0.099	0.000				0.070	0.023	5				0.070	0.023	5
px-pl.	3.866	0.032				0.115	0.025	6				0.115	0.025	6
pl	32.995	0.764				0.871	0.135	5				0.871	0.135	5
Terrestrial rock														
BCR-2	2.661	0.036										0.005	0.009	51

REFERENCES

Baker J. A., Schiller M. and Bizzarro M. (2012) 26Al-26Mg deficit dating ultramafic meteorites and silicate planetesimal differentiation in the early Solar System? *Geochim. Cosmochim. Acta* **77**, 415–431.

Barrat J. A. (2004) Determination of parental magmas of HED cumulates: the effects of interstitial melts. *Meteorit. Planet. Sci.* **39**, 1767–1779.

Barrat J. A., Blichert-Toft J., Gillet P. and Keller F. (2000) The differentiation of eucrites: the role of in situ crystallization. *Meteorit. Planet. Sci.* **35**, 1087–1100.

Barrat J. A., Yamaguchi A., Greenwood R. C., Benoit M., Cotten J., Bohn M. and Franchi I. A. (2008) Geochemistry of diogenites: still more diversity in their parental melts. *Meteorit. Planet. Sci.* **43**, 1759–1775.

Barrat J. A., Yamaguchi A., Zanda B., Bollinger C. and Bohn M. (2010) Relative chronology of crust formation on asteroid Vesta: insights from the geochemistry of diogenites. *Geochim. Cosmochim. Acta* **74**, 6218–6231.

Beck A. W. and McSween H. Y. (2010) Diogenites as polymict breccias composed of orthopyroxenite and harzburgite. *Meteorit. Planet. Sci.* **45**, 850–872.

Binzel R. P. and Xu S. (1993) Chips off of Asteroid 4 Vesta: evidence for the parent body of basaltic achondrite meteorites. *Science* **260**, 186–191.

Bizzarro M., Baker J. A., Haack H. and Lundgaard K. L. (2005) Rapid timescales for accretion and melting of differentiated planetesimals inferred from 26Al-26 Mg chronometry. *Astrophys. J.* **632**, L41–L44.

Blichert-Toft J., Boyet M., Télouk P. and Albarède F. (2002) 147Sm/143Nd and 176Lu/176Hf in eucrites and the differentiation of the HED parent body. *Earth Planet. Sci. Lett.* **204**, 167–181.

Bouvier A. and Wadhwa M. (2010) The age of the solar system redefined by the oldest Pb–Pb age of a meteoritic inclusion. *Nat. Geosci.* **3**, 637–641.

Bowman L. E., Papike J. J. and Spilde M. N. (1997) Modal Abundances in Diogenites: insights into phase percentages using electron microprobe techniques. In Lunar Planetary Science 27th. Lunar Planet. Inst., Houston.

Brennecka G. A. and Wadhwa M. (2012) Uranium isotope compositions of the basaltic angrite meteorites and the chronological implications for the early Solar System. *Proc. Natl. Acad. Sci.* **109**, 9299–9303.

Caro G., Bourdon B., Halliday A. N. and Quitté G. (2008) Superchondritic Sm/Nd ratios in Mars, the Earth and the Moon. *Nature* **452**, 336–339.

Catanzaro E. J. and Murphy T. J. (1966) Magnesium isotope ratios in natural samples. *J. Geophys. Res.* **71**, 1271–1274.

Clayton R. N. and Mayeda T. K. (1996) Oxygen isotope studies of achondrites. *Geochim. Cosmochim. Acta* **60**, 1999–2017.

Connelly J. N., Bizzarro M., Krot A. N., Nordlund Å., Wielandt D. and Ivanova M. A. (2012) The absolute chronology and thermal processing of solids in the solar protoplanetary disk. *Science* **338**, 651–655.

Consolmagno G. J. and Drake M. J. (1977) Composition and evolution of the eucrite parent body – evidence from rare earth elements. *Geochim. Cosmochim. Acta* **41**, 1271–1282.

Day J. M. D., Walker R. J., Qin L. and Rumble, III, D. (2012) Late accretion as a natural consequence of planetary growth. *Nat. Geosci.* **5**, 614–617.

Debaille V., Brandon A. D., Yin Q. Z. and Jacobsen B. (2007) Coupled 142Nd-143Nd evidence for a protracted magma ocean in Mars. *Nature* **450**, 525–528.

Drake M. J. (2001) The eucrite/Vesta story. *Meteorit. Planet. Sci.* **36**, 501–513.

Elkins-Tanton L. T., Maroon E., Krawczynski M. J. and Grove T. L. (2008) Magma ocean solidification processes on Vesta. In Lunar and Planetary Science 39th. Lunar Planet. Inst., Houston. p. #1364 (abstr.).

Elkins-Tanton L. T., Parmentier E. M. and Hess P. C. (2003) Magma ocean fractional crystallization and cumulate overturn in terrestrial planets: implications for Mars. *Meteorit. Planet. Sci.* **38**, 1753–1771.

Fowler G. W., Shearer C. K., Papike J. J. and Layne G. D. (1995) Diogenites as asteroidal cumulates: insights from orthopyroxene trace element chemistry. *Geochim. Cosmochim. Acta* **59**, 3071–3084.

Galy A., Yoffe O., Janney P. E., Williams R. W., Cloquet C., Alard O., Halicz L., Wadhwa M., Hutcheon I. D., Ramon E. and Carignan J. (2003) Magnesium isotope heterogeneity of the isotopic standard SRM980 and new reference materials for magnesium-isotope-ratio measurements. *J. Anal. At. Spectrom.* **18**, 1352.

Ghosh A. and McSween H. Y. (1998) A thermal model for the differentiation of Asteroid 4 Vesta, based on radiogenic heating. *Icarus* **134**, 187–206.

Greenwood R. C., Barrat J. A., Yamaguchi A., Franchi I. A., Scott E. R. D., Bottke W. F. and Gibson J. M. (2014) The oxygen isotope composition of diogenites: evidence for early global melting on a single, compositionally diverse, HED parent body. *Earth Planet. Sci. Lett.* **390**, 165–174.

Greenwood R. C., Franchi I. A., Jambon A. and Buchanan P. C. (2005) Widespread magma oceans on asteroidal bodies in the early Solar System. *Nature* **435**, 916–918.

Iizuka T., Yamaguchi A., Haba M. K., Amelin Y., Holden P., Zink S., Huyskens M. H. and Ireland T. R. (2015) Timing of global crustal metamorphism on Vesta as revealed by high-precision U-Pb dating and trace element chemistry of eucrite zircon. *Earth Planet. Sci. Lett.* **409**, 182–192.

Ireland T. R. and Bukovanska M. (2003) Initial ^{182}Hf/^{180}Hf in meteoritic zircons. *Geochim. Cosmochim. Acta* **132**, 259–273.

Jacobsen B., Yin Q. Z., Moynier F., Amelin Y., Krot A. N., Nagashima K., Hutcheon I. D. and Palme H. (2008) 26Al-26Mg and 207Pb-206Pb systematics of Allende CAIs: canonical solar initial 26Al/27Al ratio reinstated. *Earth Planet. Sci. Lett.* **272**, 353–364.

Jones J. H. (1984) The composition of the mantle of the eucrite parent body and the origin of eucrites. *Geochim. Cosmochim. Acta* **48**, 641–648.

Kleine T., Mezger K., Münker C., Palme H. and Bischoff A. (2004) 182Hf-182W isotope systematics of chondrites, eucrites, and martian meteorites: chronology of core formation and early mantle differentiation in Vesta and Mars. *Geochim. Cosmochim. Acta* **68**, 2935–2946.

Kleine T., Mezger K., Palme H., Scherer E. and Münker C. (2005) The W isotope composition of eucrite metals: constraints on the timing and cause of the thermal metamorphism of basaltic eucrites. *Earth Planet. Sci. Lett.* **231**, 41–52.

Kleine T., Touboul M., Bourdon B., Nimmo F., Mezger K., Palme H., Jacobsen S. B., Yin Q. Z. and Halliday A. N. (2009) Hf-W chronology of the accretion and early evolution of asteroids and terrestrial planets. *Geochim. Cosmochim. Acta* **73**, 5150–5188.

Koefoed P., Amelin Y., Yin Q.-Z., Sanborn M. E. and Huyskens M. (2015) A re-examination of the U-Pb systematics of the achondrite Asuka 881394. In Lunar and Planetary Science 46th. Lunar Planet. Inst., Houston. p. #1842 (abstr.).

Krot A. N., Keil K., Goodrich C. A. and Scott E. R. D. (2003) Classification of meteorites. In Meteorites, Comets, and Planets

Vol.1 Treatrise on Geochemistry (eds. H. D. Hollands and K. K. Turekian). Elsevier-Pergamon, Oxford. Vol. 1. pp. 83–128.

Kruijer T., Kleine T., Fisher-Gödde M., Burkhardt C. and Wieler R. (2014) Nucleosynthetic W isotope anomalies and the Hf-W chronometry of Ca-Al-rich inclusions. *Earth Planet. Sci. Lett.* **403**, 317–327.

Larsen K. K., Trinquier A., Paton C., Schiller M., Wielandt D., Ivanova M. A., Connelly J. N., Nordlund Å., Krot A. N. and Bizzarro M. (2011) Evidence for magnesium isotope heterogeneity in the solar protoplanetary disk. *Astrophys. J.* **735**, L37.

LaTourrette T. and Wasserburg G. J. (1998) Mg diffusion in anorthite implications for the formation of early solar system planetesimal. *Earth Planet. Sci. Lett.* **158**, 91–108.

Ludwig K. R. (2012) User â€TM s Manual for Isoplot 3.70, A geochronological toolkit for microsoft Excel. Berkeley Geochronol. Cent. Spec. Publ.

Lugmair G. W. and Shukolyukov A. (1998) Early solar system timescales according to 53Mn-53Cr systematics. *Geochim. Cosmochim. Acta* **62**, 2863–2886.

Mahon K. I. (1996) The New "York" regression: application of an improved statistical method to geochemistry. *Int. Geol. Rev.* **38**, 293–303.

Mandler B. E. and Elkins-Tanton L. T. (2013) The origin of eucrites, diogenites, and olivine diogenites: magma ocean crystallization and shallow magma chamber processes on Vesta. *Meteorit. Planet. Sci.* **48**, 2333–2349.

McCord T. B., Adams J. B. and Johnson T. V. (1970) Asteroid Vesta: spectral reflectivity and compositional implications. *Sci.* **168**, 1445–1447.

McSween H. Y., Binzel R. P., De Sanctis M. C., Ammannito E., Prettyman T. H., Beck A. W., Reddy V., Le Corre L., Gaffey M. J., McCord T. B., Raymond C. A. and Russell C. T. (2013) Dawn; the Vesta-HED connection; and the geologic context for eucrites, diogenites, and howardites. *Meteorit. Planet. Sci.* **48**, 2090–2104.

Misawa K., Yamaguchi A. and Kaiden H. (2005) U-Pb and 207Pb–206Pb ages of zircons from basaltic eucrites: implications for early basaltic volcanism on the eucrite parent body. *Geochim. Cosmochim. Acta* **69**, 5847–5861.

Mittlefehldt D. W. (2015) Asteroid (4) Vesta: I. The howardite-eucrite-diogenite (HED) clan of meteorites. *Chem. Erde* **75**, 155–183.

Mittlefehldt D. W. (1994) The genesis of diogenites and HED parent body petrogenesis. *Geochim. Cosmochim. Acta* **58**, 1537–1552.

Nebel O., Campbell I. H., Sossi P. A. and Van Kranendonk M. J. (2014) Hafnium and iron isotopes in early Archean komatiites record a plume-driven convection cycle in the Hadean Earth. *Earth Planet. Sci. Lett.* **397**, 111–120.

Neumann W., Breuer D. and Spohn T. (2014) Differentiation of Vesta: implications for a shallow magma ocean. *Earth Planet. Sci. Lett.* **395**, 267–280.

Nyquist L., Bogard D., Takeda H., Bansal B., Wiesmann H. and Shih C.-Y. (1997) Crystallization, recrystallization, and impact-metamorphic ages of eucrites Y792510 and Y791186 ages. *Geochim. Cosmochim. Acta* **61**, 2119–2138.

Nyquist L. E., Reese Y., Wiesmann H., Shih C. Y. and Takeda H. (2003) Fossil 26Al and 53Mn in the Asuka 881394 eucrite: evidence of the earliest crust on asteroid 4 Vesta. *Earth Planet. Sci. Lett.* **214**, 11–25.

Van Orman J. A., Cherniak D. J. and Kita N. T. (2014) Magnesium diffusion in plagioclase: dependence on composition, and implications for thermal resetting of the 26Al-26Mg early solar system chronometer. *Earth Planet. Sci. Lett.* **385**, 79–88.

Pieters C. M., Binzel R. P., Bogard D., Hiroi T., Mittlefehldt D. W., Nyquist L., Rivkin A. and Takeda H. (2006) Asteroid-meteorite links: the Vesta conundrum(s). *Proc. Int. Astron. Union* **1**, 273.

Quitté G. and Birck J. L. (2004) Tungsten isotopes in eucrites revisited and the initial 182Hf/180Hf of the solar system based on iron meteorite data. *Earth Planet. Sci. Lett.* **219**, 201–207.

Quitté G., Birck J. L. and Allègre C. J. (2000) 182Hf-182W systematics in eucrites: the puzzle of iron segregation in the early solar system. *Earth Planet. Sci. Lett.* **184**, 83–94.

Righter K. and Drake M. J. (1997) A magma ocean on Vesta: core formation and petrogenesis of eucrites and diogenites. *Meteorit. Planet. Sci.* **32**, 929–944.

Roszjar J., Whitehouse M. J., Srinivasan G., Mezger K., Scherer E. E., Van Orman J. A. and Bischoff A. (2016) Prolonged magmatism on 4 Vesta inferred from Hf–W analyses of eucrite zircon. *Earth Planet. Sci. Lett.* **452**, 216–226.

Russell C. T., Raymond C. A., Coradini A., McSween H. Y., Zuber M. T., Nathues A., De Sanctis M. C., Jaumann R., Konopliv A. S., Preusker F., Asmar S. W., Park R. S., Gaskell R., Keller H. U., Mottola S., Roatsch T., Scully J. E. C., Smith D. E., Tricarico P., Toplis M. J., Christensen U. R., Feldman W. C., Lawrence D. J., McCoy T. J., Prettyman T. H., Reedy R. C., Sykes M. E. and Titus T. N. (2012) Dawn at Vesta: testing the protoplanetary paradigm. *Science* **336**, 684–686.

Russell C. T., Raymond C. A., Jaumann R., McSween H. Y., De Sanctis M. C., Nathues A., Prettyman T. H., Ammannito E., Reddy V., Preusker F., O'Brien D. P., Marchi S., Denevi B. W., Buczkowski D. L., Pieters C. M., McCord T. B., Li J. Y., Mittlefehldt D. W., Combe J. P., Williams D. A., Hiesinger H., Yingst R. A., Polanskey C. A. and Joy S. P. (2013) Dawn completes its mission at 4 Vesta. *Meteorit. Planet. Sci.* **48**, 2076–2089.

Ruzicka A., Snyder G. A. and Taylor L. A. (1997) Vesta as the howardite, eucrite and diogenite parent body: implications for the size of the core and the large-scale differentiation. *Meteorit. Planet. Sci.* **32**, 825–840.

Sahijpal S., Soni P. and Gupta G. (2007) Numerical simulations of the differentiation of accreting planetesimals with 26 Al and 60 Fe as the heat sources. *Meteorit. Planet. Sci.* **42**, 1529–1548.

Sanborn M. E. and Yin Q.-Z. (2014) Chromium isotopic composition of the anomalous eucrites: an additional geochemical parameter for evaluating their origin. In Lunar and Planetary Science 45th. p. #2018 (abstr.).

Schiller M., Baker J. A. and Bizzarro M. (2010a) 26Al-26Mg dating of asteroidal magmatism in the young Solar System. *Geochim. Cosmochim. Acta* **74**, 4844–4864.

Schiller M., Baker J., Creech J., Paton C., Millet M.-A., Irving A. and Bizzarro M. (2011) Rapid timescales for magma ocean crystallization on the howardite-eucrite-diogenite parent body. *Astrophys. J.* **740**, L22.

Schiller M., Dallas J. A., Creech J., Bizzarro M. and Baker J. A. (2017) Tracking the formation of magma oceans in the Solar System using stable magnesium isotopes. *Geochem. Perspect. Lett.* **3**, 22–31.

Schiller M., Handler M. R. and Baker J. A. (2010b) High-precision Mg isotopic systematics of bulk chondrites. *Earth Planet. Sci. Lett.* **297**, 165–173.

Schramm N., Tera F. and Wasserburg G. J. (1970) The isotopic abundance of 26Mg and limits on 26Al in the early solar system. *Earth Planet. Sci. Lett.* **10**, 44–59.

Scott E. R. D., Greenwood R. C., Franchi I. A. and Sanders I. S. (2009) Oxygen isotopic constraints on the origin and parent bodies of eucrites, diogenites, and howardites. *Geochim. Cosmochim. Acta* **73**, 5835–5853.

Scott E. R. D. and Krot A. N. (2003) Chondrites and their components. In Meteorites, Comets, and Planets Vol.1 Treatrise on Geochemistry (eds. H. Hollands and K. Turekian). Elsevier-Pergamon, Oxford. Vol. 1. pp. 144–200.

Shearer C. K., Fowler G. W. and Papike J. J. (1997) Petrogenetic models for magmatism on the eucrite parent body – evidence from orthopyroxene in diogenites. *Meteorit. Planet. Sci.* **32**, 877–889.

Srinivasan G. (2002) 26Al-26Mg systematics in the A881394 eucrite. In Lunar and Planetary Science 33th. Lunar Planet. Inst., Houston. p. #1489 (abstr.).

Srinivasan G., Goswami J. N. and Bhandari N. (1999) 26Al in Eucrite Piplia Kalan: Plausible Heat Source and Formation Chronology. *Science* **284**, 1348–1350.

Srinivasan G., Whitehouse M. J., Weber I. and Yamaguchi A. (2004) U-Pb and Hf–W chronometry of zircons from eucrite A881467. In 35th Lunar and Planetary Science Conference. Abstract # 1709.

Srinivasan G., Whitehouse M. J., Weber I. and Yamaguchi A. (2007) The Crystallization Age of Eucrite Zircon. Science 317, 345 LP-347.

Steenstra E. S., Knibbe J. S., Rai N. and van Westrenen W. (2016) Constraints on core formation in Vesta from metal-silicate partitioning of siderophile elements. *Geochim. Cosmochim. Acta* **177**, 48–61.

Stewart B. W., Papanastassiou D. A. and Wasserburg G. J. (1994) Sm-Nd and Rb-Sr chronology and petrogenesis of mesosiderites. *Geochim. Cosmochim. Acta* **58**, 3487–3509.

Stolper E. (1977) Experimental petrology of eucritic meteorites. *Geochim. Cosmochim. Acta* **41**, 587–611.

Takeda H. (1997) Mineralogical records of early planetary processes on the howardite, eucrite, diogenite parent body with reference to Vesta. *Meteorit. Planet. Sci.* **32**, 841–853.

Takeda H. and Graham A. L. (1991) Degree of equilibration of eucrite pyroxenes and thermal metamorphism of the earliest planetary crust. *Meteorit. Planet. Sci.* **26**, 129–134.

Tang H. and Dauphas N. (2012) Abundance, distribution, and origin of 60Fe in the solar protoplanetary disk. *Earth Planet. Sci. Lett.* **359–360**, 248–263.

Touboul M., Sprung P., Aciego S. M., Bourdon B. and Kleine T. (2015) Hf-W chronology of the eucrite parent body. *Geochim. Cosmochim. Acta* **156**, 106–121.

Treiman A. H. (1997) The parent magmas of the cumulate eucrites: a mass balance approach. *Meteorit. Planet. Sci.* **32**, 217–230.

Trinquier A., Birck J. L., Allègre C. J., Göpel C. and Ulfbeck D. (2008) 53Mn-53Cr systematics of the early Solar System revisited. *Geochim. Cosmochim. Acta* **72**, 5146–5163.

Wadhwa M., Amelin Y., Bogdanovski O., Shukolyukov A., Lugmair G. W. and Janney P. (2009) Ancient relative and absolute ages for a basaltic meteorite: implications for time-scales of planetesimal accretion and differentiation. *Geochim. Cosmochim. Acta* **73**, 5189–5201.

Walker F. W., Parrington J. R. and Feiner F. (1989) Nuclides and Isotopes, 14th ed. General Electric Co. 57 pp.

Warren P. H., Rubin A. E., Isa J., Gessler N., Ahn I. and Choi B. G. (2014) Northwest Africa 5738: multistage fluid-driven secondary alteration in an extraordinarily evolved eucrite. *Geochim. Cosmochim. Acta* **141**, 199–227.

Wasserburg G. J., Wimpenny J. and Yin Q.-Z. (2012) Mg isotopic heterogeneity, Al-Mg isochrons, and canonical 26Al/27Al in the early solar system. *Meteorit. Planet. Sci.* **47**, 1980–1997.

Wasson J. T. (2013) Vesta and extensively melted asteroids: why HED meteorites are probably not from Vesta. *Earth Planet. Sci. Lett.* **381**, 138–146.

Williams C. D., Sanborn M. E. and Yin Q.-Z. (2015) Ti-Cr-O isotope systematics of the anomalous eucrites and martian meteorites. In Lunar and Planetary Science 46th. Lunar Planet. Inst., Houston. p. #1671 (abstr.).

Wimpenny J., Yin Q. Z. and Amelin Y. (2011) Vesta's primorpdial differentiation as revealed by 26Al-26Mg isotope systematics of bulk eucrites and diogenites. In Formation of the First Solids in the Solar System p. #9075 (abstr.).

Wimpenny J., Yin Q. Z., Cooke I., Stirling C. and Amelin Y. (2013) Reassessing the chronology of the unique achondrite asuka 881394 using Al-Mg and U-Pb systematics. In Lunar and Planetary Science Conf. 44th. Lunar Planet. Inst., Houston. p. #2308 (abstr.).

Yamaguchi A., Barrat J. A., Greenwood R. C., Shirai N., Okamoto C., Setoyanagi T., Ebihara M., Franchi I. A. and Bohn M. (2009) Crustal partial melting on Vesta: evidence from highly metamorphosed eucrites. *Geochim. Cosmochim. Acta* **73**, 7162–7182.

Yamaguchi A., Barrat J. A., Ito M. and Bohn M. (2011) Posteucritic magmatism on Vesta: evidence from the petrology and thermal history of diogenites. *J. Geophys. Res. E Planets* **116**, E08009.

Yamaguchi A., Setoyanagi T. and Ebihara M. (2006) An anomalous eucrite, Dhofar 007, and a possible genetic relationship with mesosiderites. *Meteorit. Planet. Sci.* **41**, 863–874.

Yamaguchi A., Taylor G. J. and Keil K. (1996) Global crustal metamorphism of the eucrite parent body. *Icarus* **124**, 97–112.

Yamaguchi A., Taylor G. J. and Keil K. (1997) Metamorphic history of the eucritic crust of 4 Vesta. *J. Geophys. Res.* **102**, 381–386.

Zhou Q., Yin Q.-Z., Young E. D., Li X.-H., Wu F.-Y., Li Q.-L., Liu Y. and Tang G.-Q. (2013) SIMS Pb–Pb and U–Pb age determination of eucrite zircons at 5 μm scale and the first 50 Ma of the thermal history of Vesta. *Geochim. Cosmochim. Acta* **110**, 152–175.

Associate editor: Dimitri A. Papanastassiou